Techniques for ground moving target detection and velocity estimation with multi-channel Synthetic Aperture Radars (SAR)

Davide Rizzato

Aprile 2012

alla mia famiglia

Contents

List of Figures

List of Tables

Introduction

What today is known as Synthetic Aperture Radar -SAR- was invented by Carl Atwood Wiley in the 1965 [1]. Nowadays this technology has improved a lot and is widespread. In the last decade the interest in it is particulary oriented towards its use in satellite mission for mapping the Earth's surface and remote sensing purpose.

SAR satellites are used in different applications from topographic mapping to polar ice research. Moreover for studies of ocean currents or military surveillance [2][3]. Traditionally SAR systems form images of the observed scene but nowadays the challenge is to use this technology to detect moving targets in the Earth's surface, like boats in a sea scenario or road traffic in suburban area. In order to do so techniques that allow detecting moving targets from the background static scene, also called clutter. With the aim to build a complete system for traffic surveillance, it is required also an estimation of the velocity vector of these moving target. An important feature of these satellites, working at the microwave band of the electromagnetic spectrum, is that they could operate also during night and in adverse weather conditions.

At present, there are a lot of active SAR satellite missions, for example the Canadian and the German have the RADARSAT-2 [4] and TERRASAR-X [5] satellites, respectively. Moreover, the Italian COSMO-SkyMed [6] system is based on a constellation of four satellites that was completed with the last launch in 2010. In the near future Spain will also contribute with the launch of SEOSAR/PAZ [7]. It is important to note that none of these SAR satellites was optimized for Ground Moving Target Indication (GMTI) but nevertheless experimental GMTI modes can be operated as the case of MODEX in RADARSAT-2 mission [8].

The frame of this thesis is the application of SAR for maritime surveillance. The Mediterranean sea has been the theater of intense illegal immi-

gration phenomena; in the last decade the number of boats arrivals is rising at growing rate [9]. Unfortunately, these journeys can end up in tragedies. In this context there has been an increasing interest within the European borders to use SAR technology for monitoring purposes [10]. Furthermore the possibility to have satellites with this capability could aid in other problems connected with maritime scenario, such as piracy prevention and illegal traffics (arms, toxic waste, etc).

This thesis is made in collaboration with the Department of Signal Theory and Communications (TSC) of the Universitat Politècnica de Catalunya (UPC). This Department participates in the NEWA (New European WAtcher) [10] project founded by the European Community. NEWA is focussed on techniques and technology development in the ground moving target indication framework. In the UPC is being developed a complete simulator tool for SAR-GMTI, from raw data generation to target detection and estimation.

Thesis objectives

The main objective of this thesis is the study and implementation in the UPC-SAR simulator of a relatively new detection and velocity estimation technique for moving targets in sea scenarios. A Constant False Alarm (CFAR) detector based on fractional Fourier transform[1] and on Displaced Phase Center Antenna (DPCA) has been implemented. For velocity estimation Along-Track interferometry (ATI) and, again, the fractional Fourier transform are used.

Current SAR missions are limited by two physical receiver chains. Additional virtual channels can be obtained, keeping the hardware configuration of two channels, by means of programming of the antenna in receive and/or transmit. These modes of operation, originally proposed in the frame of RADARSAT-2 [11], have been implemented and integrated in the simulator within the frame of this thesis. The aim of the thesis is to understand through simulations if such a technique provides improved velocity estimation combined with the detection based on the fractional Fourier transform.

The final purpose of this thesis is the evaluation of the new methods implemented in the UPC-SAR-GMTI simulator through simulation carried out considering different sea conditions and for different types of modeled boats.

[1]Fractional Fourier transform is a generalization of the classical Fourier transform.

Thesis organization

The thesis begins introducing the basic principles of radars: the satellite-Earth geometry is described and Synthetic Aperture Radar is defined in chapter 1.

In chapter 2 the study of the characteristics of the pulse transmitted and received by the SAR is described jointly with a brief introduction to SAR processing, which is required to form focused images.

The definition of the Ground Moving Target Indication (GMTI) systems in relation to the moving target signal model and the characterization of sea clutter are given in the first part of chapter 3. This chapter follows with the basic principles on classical tools used for clutter suppression, DPCA, and velocity estimation, ATI. Antenna toggle modes for virtual channel creation are also delineated.

In the first part of chapter 4 the detection technique proposed using DPCA and fractional Fourier transform is illustrated. In the successive section the velocity estimation technique is described. In the final section of chapter 4 the detailed scheme of the proposed procedure, to be integrated in the UPC simulator, is presented.

The simulations for different sea conditions and different type of targets are presented in chapter 5, providing performance metrics in terms of probability of detection and velocity estimation error.

Chapter 5.4 summarizes the contributions of the thesis in line with some conclusions and provides general hints for future work.

Chapter 1

Principles of radar and synthetic aperture

This chapter is intended to provide the reader with some basic principles on radar in order to understand the concept behind the so called synthetic aperture radar. It begins illustrating the basic geometry of a spaceborne radar, follows explaining the linear frequency modulation and ends illustrating the synthetic aperture idea.

1.1 Spaceborne radar geometry

The geometry of a spaceborne radar and the footprint of the antenna beam are shown in figure 1.1. Below are introduced some terms used throughout all this thesis.

Point target: The radar system is imaging a strip in the Earth's surface, in order to explain the basic theory is considered throughout this chapter a single stationary point target.

Beam footprint: This is the projection of the radar antenna beam onto the ground.

Nadir: Point in the Earth's surface perfectly below the radar; rigorously, the nadir is originated by the intersection between the normal to the Earth's surface and the satellite.

Incidence angle θ_i: Angle between the radar beam and the local normal to the ground that crosses the target.

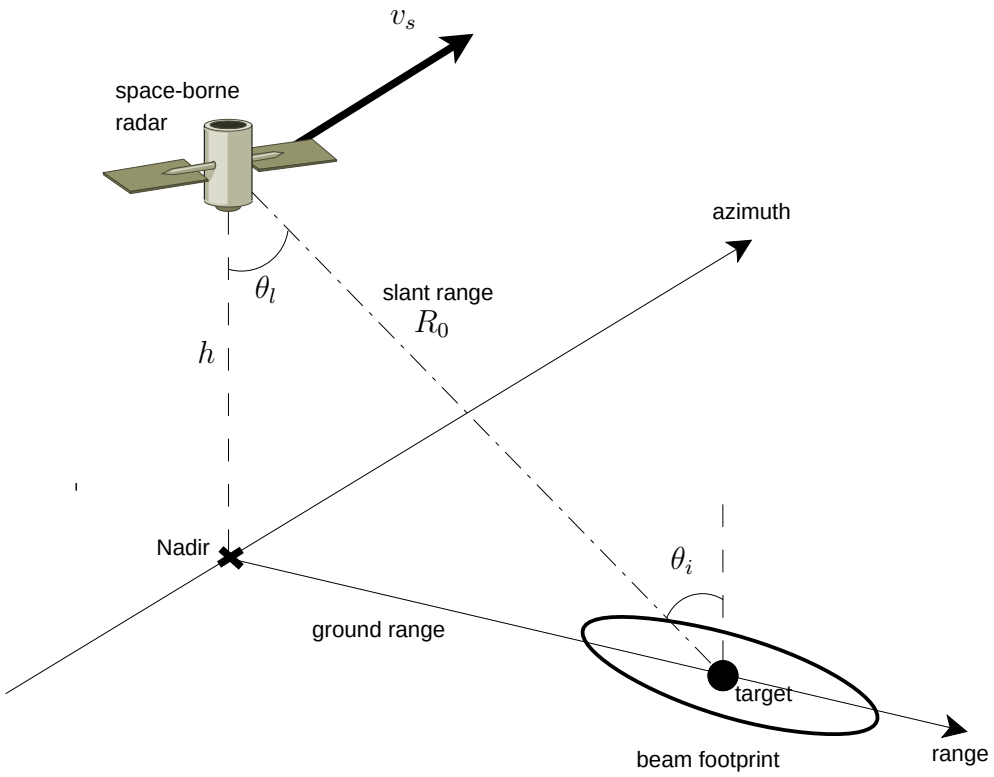

Figure 1.1: Spaceborne radar and antenna beam footprint geometry.

Look angle θ_l: Angle between the vertical to the ground that crosses the nadir and the radar beam.

Azimuth axis: Axis aligned with the satellite track. The azimuth time is indicated by t.

Range axis: This is the axis orthogonal to the azimuth one. The range time is expressed by u.

Slant range: This is the time-variable distance from the radar to the target.

Ground range: This is the projection of slant range onto the ground.

Radial velocity v_r: Target's velocity seen by the radar along the direction of the line of sight.

Zero Doppler plane: Is the plane originated when the relative radial velocity of the radar with respect to the target is zero. It is normal to the satellite track and crosses the target.

Target trajectory: Trajectory that arises from the apparent movement of the target caused by the flight of the satellite. It is plotted in the azimuth-range axes.

Range of closest approach R_0: Range when the zero Doppler plane crosses the target and the range is at minimum. The time of closest approach t_0 is called **Zero Doppler time**.

Side-looking configuration: The radar antenna illuminates a surface strip to one side of the nadir track. Hypothetically, if the radar looks straight to the ground in a non side-looking configuration, ambiguities left-right would arise from two symmetric equidistant points.

Target exposure time: This parameter express how long the target stays in the antenna beam (in the -3 dB limit).

In the above definitions of terms, in the figure 1.1 and throughout all the text some simplifications from a real scenario have been made.

It is considered a local flat model of the Earth and a locally straight flight path of the satellite, moreover the center of the beam of the antenna is considered perfectly normal to the flight path. The complete description of the problem goes beyond the needs of this thesis, it would be only a generalization of the concepts presented above, for a more detailed description see reference [12].

Assuming a local flat model for the Earth and straight flight path, the satellite velocity and the antenna beam velocity at the ground are are the same. Moreover incident and look angles, θ_l and θ_i, are complementary.

1.2 Radar basic concepts

Let us consider a basic radar system that transmit a signal $s_{sin}(u)$ which is a sinusoidal pulse of length T with f_0 carrier frequency.

$$s_{sin}(u) = \cos(\omega_0 u) \text{ for } -\frac{T}{2} < u < \frac{T}{2} \tag{1.1}$$

where $w_0 = 2\pi f_0$.

It's possible to take, in general, the bandwidth B_p of a sinusoidal pulse as

$$B_p = \frac{1}{T} \tag{1.2}$$

therefore, long sinusoidal pulses have a narrow bandwidth, vice versa short pulses have a wide bandwidth.

The bandwidth of a pulse is of central importance in radar system because is related to the resolution in the range direction and hence directly to the capability to discriminate neighboring targets.

Let us consider two point targets separated, in range, by a distance Δd. The two echoes at radar receiver will be separated by a time $\Delta u = \frac{2\Delta d}{c}$. In order for the two echoes not to overlap at the receiver, it's necessary that the pulse duration is $T < \frac{2\Delta d}{c}$.

Range resolution Δ_r can be defined as the shortest separation Δd that can be measured by the radar, that is

$$\Delta_r = \Delta d = \frac{cT}{2} = \frac{c}{2B} \tag{1.3}$$

Thus, in order to get small Δ_r, namely high resolution, a wide bandwidth or a short pulse is needed.

The length of the pulse is directly connected to the pulse energy that is

$$E = P_p T \ , \tag{1.4}$$

where P_p is the instantaneous peak power. Generally is desired a high energy pulse in order to detect weak target, from (1.4) is clear that this can be done by increasing the pulse duration T or the peak power P_p.

On one side the maximum power is limited by radar hardware, on the other side, as discussed before, a longer pulse corresponds to a narrower bandwidth and hence a worse range resolution. The aim is to have high energy E (large pulse duration) and high resolution (large bandwidth), this is achieved by modulating the pulse.

1.2.1 Chirp: linear frequency modulation

Linear frequency modulation (FM) is one of the most common pulse modulation schemes, a pulse with this characteristic is called chirp. The frequency f_0 changes linearly from f_0 to $f_0 + \Delta f$ during the pulse duration. Note that the bandwidth B_c, in this case, is independent of the pulse length T, and is equal to

$$B_c = (f_0 + \Delta f) - f_0 = \Delta f \tag{1.5}$$

Hence a pulse with large duration and large bandwidth can be built.

The mathematical expression of the chirp used in the UPC-SAR simulator is

$$s_{tx}(u) = \cos\left(2\pi f_0 u + \pi K_r u^2\right) \text{ for } -\frac{T}{2} < u < \frac{T}{2} \tag{1.6}$$

where K_r is the rate of the frequency modulation, T is the pulse duration and f_0 is the carrier frequency.

The benefit of using a chirp lies in the possibility to compress it at the receiver. Therefore, a chirp of long duration can achieve high range resolution equivalent to a short duration pulse. At reception a properly matched filter compress the total energy into a much shorter pulse.

The spectrum of a linear FM signal has a quadratic phase. In the frequency domain this spectrum is multiplied by a filter that has the conjugate quadratic phase of the input signal, the result is a flat phase. Finally, the inverse Fourier transform gives a time compressed signal. The terminology of matched filter arises from the fact that the filter is adapted to the expected phase of the signal.

The length of the output pulse T' is limited by the bandwidth B_c to

$$T' = \frac{1}{B_c} = \frac{1}{\Delta f}.$$

It's important to observe that before compression the echoes from two neighboring targets might be overlapped in time, nevertheless the separation of the echoes can be obtained considering that the instantaneous frequencies from each echo at a same time are different.

1.3 Synthetic Aperture Radar - SAR

To understand why is need a Synthetic Aperture Radar (SAR) for high resolution imaging system is necessary to introduce the concept of azimuth resolution for real aperture radar. Following a similar way as the definition of the range resolution given in section 1.2 is possible to say that the resolution in azimuth corresponds to the two nearest separable point targets along an azimuth line.

Real aperture radar

The concept of azimuth resolution is related to the width in azimuth of the antenna footprint, in fact all the pulses from different azimuth positions, but with the same range, reach the receiver at the same time. The azimuth resolution for real aperture radar is:

$$\Delta'_a = \frac{R_0 \theta'_a}{cos(\theta_l)} \tag{1.7}$$

where R_0 is the slant range defined in 1.2, θ'_a is the azimuth antenna beamwidth and θ_l is the look angle.

Considering the wavelength λ and the length L of the antenna beamwidth can be approximated by

$$\theta'_a = \frac{\lambda}{L}. \tag{1.8}$$

It's easy to show how, with typical parameters, the azimuth resolution θ'_a is in the order of kilometers and, hence, too low for imaging applications.

For example, let us consider $R_0 = 500$ km , $\lambda = 30$ mm , $L = 5$ m and $\theta_l = 45°$ follow that the azimuth resolution is equal to $\Delta'_a = 4.2$ km .

A meaningful solution to improve the azimuth resolution seem to increase the antenna length L, however it's obvious that a satellite can't board an extremely huge antenna; therefore a synthetic aperture technique is used.

Azimuth resolution for SAR

The basic idea of SAR is to add coherently successive echoes received throughout the satellite's flight, the result is to synthesize a linear antenna array. Assuming a length L for the radar's antenna, the synthetic aperture L_s is defined as the azimuth length of the antenna main beam footprint on the Earth's surface, look at figure 1.2,

$$L_s = R_0\theta'_a = R_0\frac{\lambda}{L} \ . \tag{1.9}$$

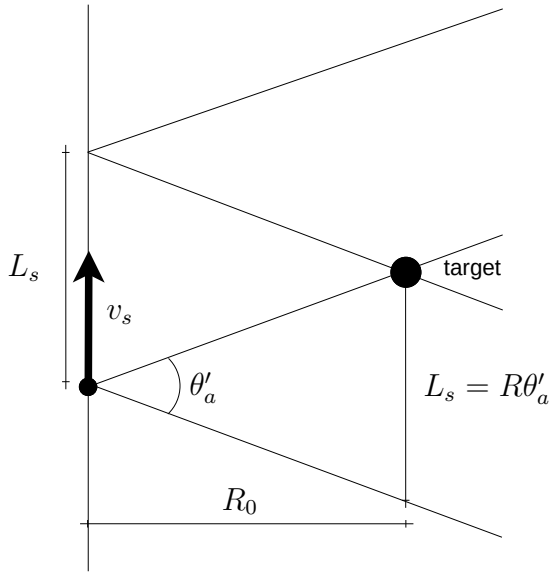

Figure 1.2: Syntectic aperture length L_s definition.

Analogously to (1.8) the beam width θ_s of the synthetic aperture is given by

$$\theta_s = \frac{\lambda}{2L_s} = \frac{L}{2R_0} \tag{1.10}$$

where the factor of two accounts for the two-way path of the radar signal. Finally, it is possible to find the azimuth resolution Δ_a using a synthetic aperture technique as

$$\Delta_a = R_0\theta_s = \frac{L}{2}. \tag{1.11}$$

Referring to the previous example where was found a real aperture azimuth resolution of $\Delta'_a = 4.2$ km , in the case of SAR, with the same antenna length, $L = 5$ m, using (1.11) the azimuth SAR resolution is $\Delta_a = 2.5$ m, improved by orders of magnitude with respect to $\Delta'_a = 4.2$ km.

From (1.11) is shown that the resolution is independent from the distance between radar and target, and also that finer resolution can be achieved with smaller antennas. However is important to taking into account that the signal-to-noise ratio, in a real condition of satellite power limitation, place a lower limit on the antenna size.

1.4 The range equation

The distance, or range, from the SAR to the target changes as the satellite flies; when the sensor approaches the target the range decreases, on the contrary, when it goes away the range increases.

To express the range equation is considered a geometry like the one in figure 1.3.

Let us consider a satellite velocity of v_s, the distance D is given by

$$D = v_s t \tag{1.12}$$

where t is the azimuth time. The time reference is the time of closest approach t_0 defined in section 1.1.

Using the Pythagorean theorem is found the hyperbolic form of the range equation $R(t)$ that is equal to

$$R^2(t) = R_0^2 + D^2 = R_0^2 + v_s^2 t^2 \tag{1.13}$$

where R_0 is the range of closest approach defined in section 1.1.

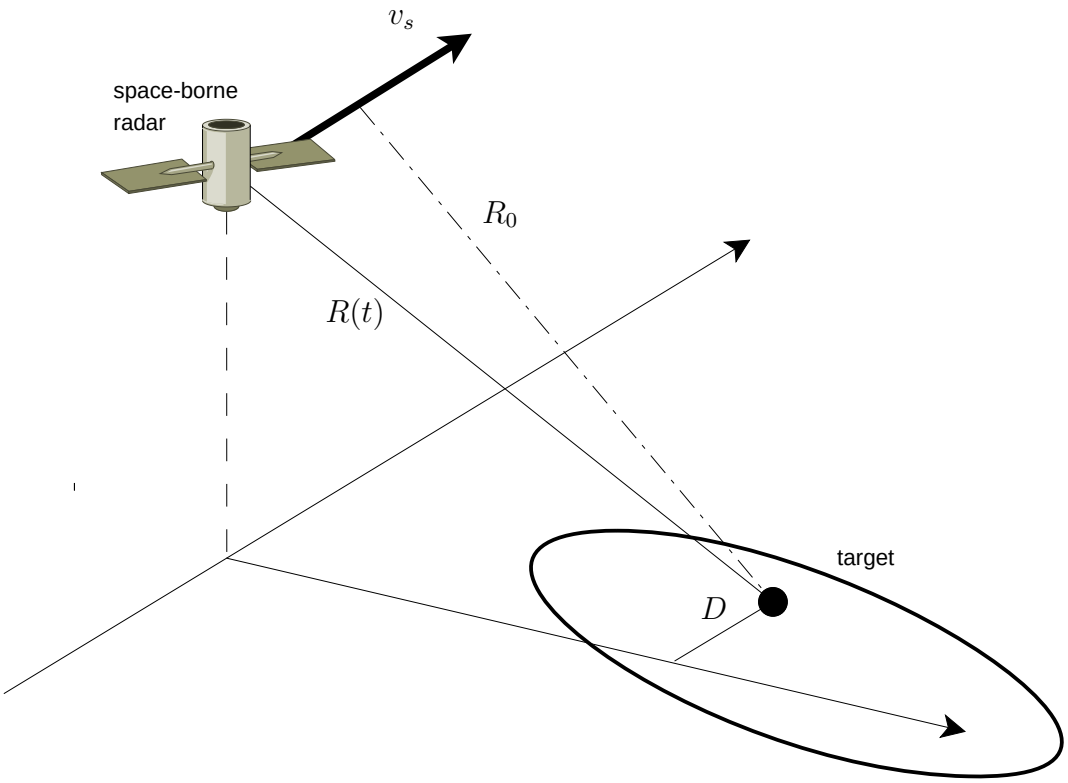

Figure 1.3: Time variable range $R(t)$ and distance D geometry.

Chapter 2

Pulse characteristics and SAR processing

This chapter illustrates the signals involved in a synthetic aperture radar, both in range and azimuth direction. At the end of this chapter, a processing SAR algorithm is shortly described.

2.1 SAR signal

It is possible to describe first the SAR signal in the range and azimuth coordinates separately and, in a second step, the coupling between the signals is included in the two dimensional space. The range distance is related to range time u by the speed of light, hence the range time is called "fast time"; on the other hand the azimuth time t is associated with the motion of the satellite along is flight path and is called "slow time".

2.1.1 Range direction

The radar emits, in the range direction, a chirp as described in section 1.2.1, the signal is reported here

$$s_{tx}(u) = \cos\left(2\pi f_0 u + \pi K_r u^2\right) \text{ for } -\frac{T}{2} < u < \frac{T}{2}. \tag{2.1}$$

Let us consider a stationary point target at a distance R from the SAR, where the constant A' includes the common mode parameters as the backscattering coefficient, propagation losses and antenna patterns. The time delay of the signal for that target is $2R/c$, therefore the signal received from the point target is

$$\begin{aligned} s_r(u) &= A' s_{tx}\left(u - \frac{2R}{c}\right) \\ &= A' w_r\left(u - \frac{2R}{c}\right) \cos\left[2\pi f_0\left(u - \frac{2R}{c}\right) + \pi K_r\left(u - \frac{2R}{c}\right)^2 + \psi\right] \end{aligned} \tag{2.2}$$

where ψ accounts for a possible phase change caused by the scattering process from the surface; ψ is considered constant through all the satellite flight. In (2.2) the function $w_r(u)$ is the rectangular pulse envelope

$$w_r(u) = rect\left(\frac{u}{T}\right). \tag{2.3}$$

2.1.2 Azimuth direction

During the flight of the satellite the SAR transmits and receives subsequent pulses. The time elapsed between the transmission of two chirps is called Pulse Repetition Interval - PRI. Then, the Pulse Repetition Frequency is PRF=1/PRI.

Doppler frequency consideration

It is important to understand that the echo from a stationary point target is affected by a Doppler frequency shift caused by the relative speed of the SAR with respect to the target. When the distance from the satellite to the target is decreasing, the frequency of the received echo increases and, vice versa, when the SAR antenna goes away from the target the frequency decreases. Hence, the relative motion between the platform and the fixed target produces a linear frequency modulation as the one used in TX pulse (chirp).

The spectrum of the signal received from a stationary point target covers the region $f_0 \pm f_D$ where f_D is equal to

$$f_D = -\frac{2}{\lambda} v_r = \frac{2}{\lambda} v_s \sin\left(\frac{\theta'_a}{2}\right) \simeq \frac{v_s \theta'_a}{\lambda} = \frac{v_s}{L}\ , \tag{2.4}$$

where v_r is the relative speed between the radar and the target (figure 2.1) and in the last step is used the approximation (1.8). It's obvious that the Doppler bandwidth is

$$B_D = 2 f_D = \frac{2 v_s}{L}. \tag{2.5}$$

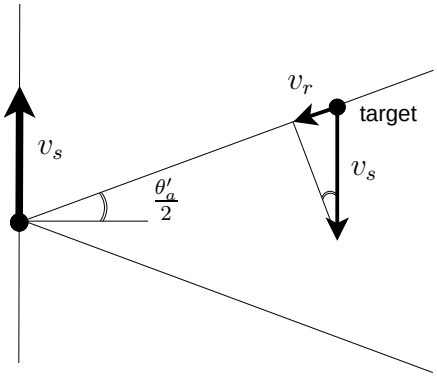

Figure 2.1: Radial velocity v_r at the edge of the azimuth beam.

The relative motion produces a linear frequency modulation of the signal in the azimuth dimension, with a bandwidth characterized by the B_D and sampled at each acquisition instant determined by the PRF.

As it can be seen from the figure 2.2 the received signal strength is governed by the azimuth antenna pattern $p_a(\theta)$, more precisely by the two-way antenna pattern. Note that the angle θ is a function of azimuth time t.

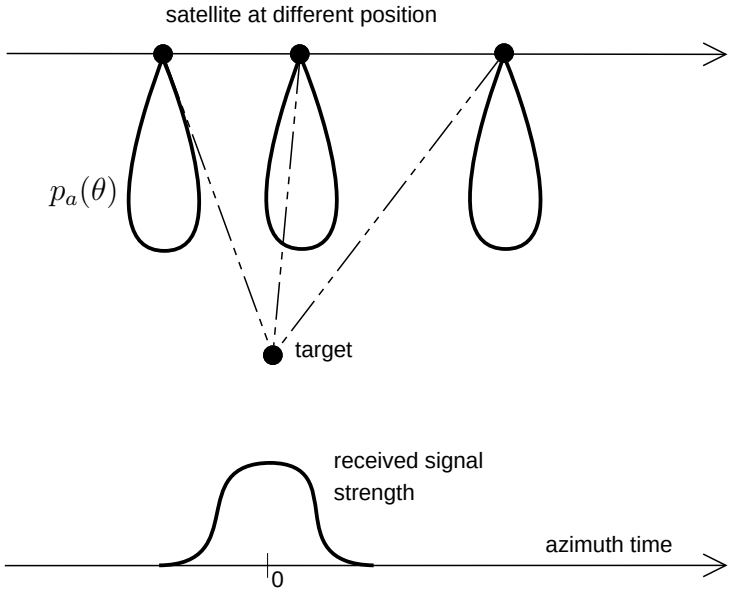

Figure 2.2: Received signal strength caused by antenna pattern $p_a(\theta)$ as a function of the azimuth time t.

The signal received from the target as a function of range time u and azimuth t is

$$\begin{aligned} s_r(u,t) &= A' w_r\left(u-\frac{2R(t)}{c}\right) p_a^2(\theta(t)) \times \\ &\quad \times \cos\left[2\pi f_0\left(u-\frac{2R(t)}{c}\right)+\pi K_r\left(u-\frac{2R(t)}{c}\right)^2+\psi\right], \end{aligned} \tag{2.6}$$

where for $R(t)$ is considered the range equation (1.13) that model the azimuth-time dependent slant range distance from the SAR to the target as the satellite flies.

2.1.3 Baseband two-dimensional received signal

After the demodulation process of the received signal the baseband representation can expressed as

$$\begin{aligned} s_0(u,t) &= A w_r\left(u-\frac{2R(t)}{c}\right) p_a^2(\theta(t)) \times \\ &\quad \times \exp\left[-j4\pi f_0\frac{R(t)}{c}\right] \exp\left[j\pi K_r\left(u-\frac{2R(t)}{c}\right)^2\right] \end{aligned} \tag{2.7}$$

that represents the demodulated two-dimensional baseband signal, where now the coefficient A is a complex costant given by

$$A = A' e^{j\psi}. \tag{2.8}$$

Hereafter the signal in (2.7) is referred also as "raw data" signal.

Reviewing of the SAR signal operation

The radar samples the continuous-time echo received from a transmitted chirp scattered by a target, these samples are saved along the range axis. Moving along its flight path, SAR emits pulses in accordance with the PRF. Therefore, the signal saved in azimuth axis is already in discrete-time, that samples are taken exactly at the Pulse Repetition Frequency.

Pulse repetition considerations

PRF is a key parameter in the design of the SAR systems and should be carefully analyzed. The PRF should be high enough to ensure that the

Doppler bandwidth B_D (2.5) is sufficiently well sampled in order to avoid ambiguities. That is

$$\text{PRF} > B_D = \frac{2v_s}{L} \ . \tag{2.9}$$

On the other hand, no more than one pulse may fall in the surface footprint at any instant of time, otherwise, echoes from two different pulses and different areas will be received at the same time. In other words successive pulses have an upper limit in terms of PRF,

$$\text{PRF} < \frac{c}{2R_s} \tag{2.10}$$

where $R_s = R_{max} - R_{min}$, as it could be seen in figure 2.3.

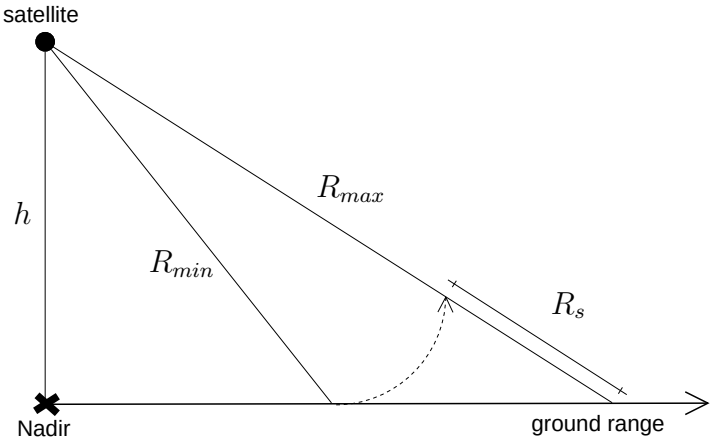

Figure 2.3: Definition of the maximum R_{max} and minimum R_{min} range and their difference R_s used in the calculation of the upper limit of the PRF.

2.1.4 Approximations

It is useful to make some approximations. It is possible to obtain a parabolic approximation of the hyperbolic range equation (1.13), that is

$$R(t) = \sqrt{R_0^2 + v_s^2 t^2} \approx R_0 + \frac{v_s^2 t^2}{2R_0}. \tag{2.11}$$

The baseband received signal (2.7) can now be approximated by

$$s_0(u,t) \approx A w_r \left(u - \frac{2R(t)}{c}\right) p_a^2(\theta(t)) \exp\left[-j\frac{4\pi R_0}{\lambda}\right] \times$$

$$\times \exp\left[-j\pi K_a t^2\right] \exp\left[j\pi K_r \left(u - \frac{2R(t)}{c}\right)^2\right] \qquad (2.12)$$

where the azimuth FM rate K_a is the rate of change of azimuth (i.e. Doppler) frequency and is given by

$$K_a = \frac{2v_s^2}{\lambda R_0}. \qquad (2.13)$$

Observe that the azimuth frequency modulation is linear (quadratic in phase) as in the range dimension modulation. Similarly to the case of the range signal, is possible to compress the azimuth signal through a matched filter and obtain the SAR azimuth resolution found in (1.11).

2.2 Processing of SAR signal

The signal received by the synthetic aperture radar must be processed in order to obtain a focused image. Before giving an overview of the algorithm used in the UPC-SAR simulator is necessary to explain the frequency or time domains involved in the processing and the concept of range cell migration.

If is considered the range time and azimuth frequency the domain is called "range Doppler", since the azimuth frequency is synonymous with Doppler frequency. The other domain of interest is the two-dimensional, range and azimuth, frequency domain.

As was said earlier, during the formation of the synthetic aperture, the range between the sensor and a certain target varies; plotting the range of the received echo from a target versus azimuth time is obtained a parabolic curve that crosses several range cells. This is called Range Cell Migration (RCM) and must be compensated to obtain either the compression of the energy into a single point and high resolution.

2.2.1 Range-Doppler Algorithm - RDA

The range Doppler algorithm (RDA) was developed in the 70s and is still the most commonly used algorithm for processing SAR raw data into an image [12].

In the range Doppler domain, adopted by RDA, all targets having the same slant range of closest approach are collapsed into one single trajectory, as shown in figure 2.4. In fact, to transform the data to the range Doppler domain, an azimuth Fourier transform is performed, and by virtue of the Fourier transform time shift theorem the energy of all these targets will be placed in the same frequency samples.

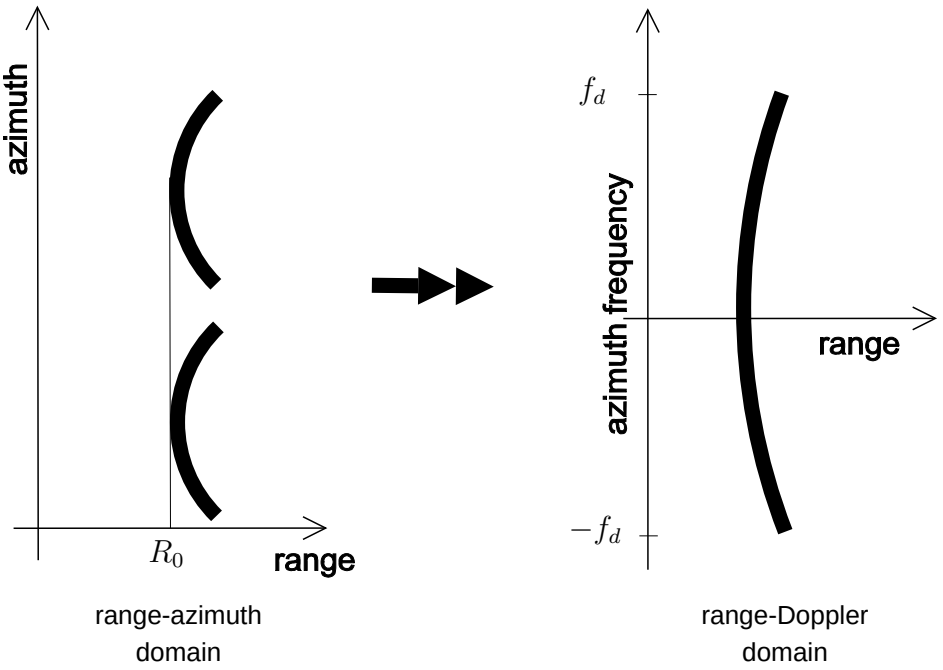

Figure 2.4: Collapsing of multiple targets with same slant range into one trajectory in range-Doppler domain.

RDA is computationally efficient exactly because the correction of one target trajectory (Range Cell Migration Correction - RCMC) in the range Doppler domain corrects a family of target trajectories, the ones having the same slant range of closest approach. Moreover, all the matched filter convolutions are performed as complex multiplications in the frequency domain. RDA also decouples the 2-dimensional processing into a two steps 1-dimensional elaboration, first in range and second in azimuth direction.

In figure 2.5 is shown the block diagram of the basic RDA algorithm.

Range compression is performed by range Fast Fourier Transform FFT followed by a range matched filter multiplication and finally a range inverse FFT.

Azimuth FFT allows to bring the data into the data into the range Doppler domain.

RCMC is performed in the range Doppler domain, the effect of RCMC is to concentrate the energy of targets over the same range cell bin, the one of closest approach, in order to maximize the response of the target with the specific azimuth resolution.

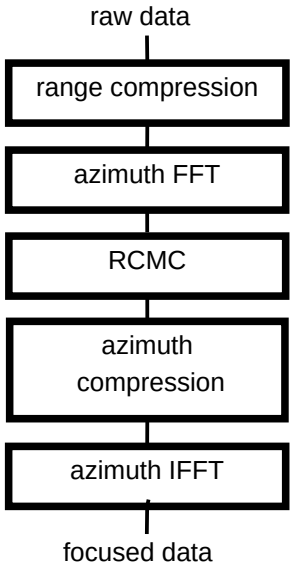

Figure 2.5: Block diagram of the range Doppler algorithm.

Azimuth compression is performed by an azimuth matched filtering implemented in the frequency domain as a multiplication.

Azimuth IFFT In this final step is involved an inverse fast Fourier transform in order to return in the range azimuth times domain.

Finally, compressed data are given in a complex focused image where moving target detection can be performed.

Chapter 3

Multi-channel SAR and moving target detection

In the previous chapter are outlined the principles of the synthetic aperture radars and the processing of raw data to form focused images of the scenes observed by a spaceborne SAR. However if it's wanted to detect moving targets is necessary to introduce also others basic principles and techniques. This thesis focuses on the detection of moving ships in a sea background.

This chapter describes basic principles on Ground Moving target Indication (GMTI), considering the signal model characterization of a moving target observed by a SAR. Two GMTI techniques are briefly described, Displaced Phase Center Antenna (DPCA) and Along-Track Interferometry (ATI). At the end of this chapter is illustrated a way to obtain three or more virtual channels maintaining the hardware system complexity, i.e. keeping the limitation of two single physical available channels as the case of RADARSAT-2 or SEOSAR/PAZ.

3.1 Ground Moving Target Indication (GMTI)

Historically radar ground systems were used to detect moving targets for defense purposes, for example, detecting approaching ships or enemy aircrafts. It refers to these as Moving Target Indication (MTI) systems. Actually, the aim of MTI radars wasn't to form images, but to cancel signals from fixed or slow-moving scatterers such as buildings, hills or sea to maintain the information of moving targets only.

The principle behind MTI was to use the Doppler shift in the received echoes in order to distinguish moving targets from clutter, since this spectral

displacement is related to the velocity of the target in the range direction [15].

MTI in spaceborne systems is much more complicated compared to the fixed ground radars since the platform that carries the radar also induced a Doppler spectrum on the fixed scene, as seen in 1.

The challenge, hence, is to build a satellite SAR system which owns Ground Moving Target Indication (GMTI) techniques. On one side the Doppler shift induced by the relative movement between the platform and the fixed scene is the property which is exploited to form the synthetic aperture, but on the other side, is impossible to distinguish the Doppler shift of a moving target from the one of the clutter. The conclusion is that is necessary a system that cancel the clutter. In fact, with single channel SAR systems it is possible to detect moving targets only if their velocity is high enough that they come out from the clutter spectrum. Two channels SAR configurations provide additional diversity that can be exploited either to cancel out the clutter or estimate the target velocity [16], with more than two channels there are more degrees of freedom, both cancel clutter and estimate the velocity could be possible.

3.2 Characterization of sea clutter

Depending on which radar application is treated, exist different definitions of clutter. In the case of this thesis (SAR-GMTI) clutter is the scene background, i.e. sea surface, which competes with the moving targets of interest.

In this thesis a preliminary sea clutter model (implemented in the UPC SAR-MTI simulator) has been considered. In this case, the clutter is characterized by a collection of point-like scatterers, with more than one per resolution cell, whose reflectivity follows a circular complex Gaussian distribution. Temporal decorrelation has been also included in the model [20].

The UPC SAR-MTI simulator is being updated with a more realistic sea clutter model based on a K-distribution as suggested in [21].

For this thesis the mean reflectivity coefficient σ_0 for the Gaussian distribution is extrapolated from the work carried out by Nathanson et al. in [22] for the X-band frequency of interest. The temporal decorrelation τ_c that agree with the temporal decorellation of the sea surface [23] is approximated by

$$\tau_c \cong 3\frac{\lambda}{u} erf^{-1/2}\left(2,7\frac{x}{u^2}\right) \ , \tag{3.1}$$

where u is the wind speed, x is the spatial resolution in ground range and

$erf()$ is the Gauss error function. The sea specifications are in agreement to the World Meteorological Organization sea state code [24] and the Beaufort wind scale [25].

3.3 Dual Receive Antenna (DRA) mode

In single-channel SAR data, there is an ambiguity in the Doppler signature of an object, Doppler shift could be due to the position of the scatterer in the antenna beam, or to its movement.

This intrinsic ambiguity between azimuth position and radial velocity can be solved by means of additional spatial diversity, i.e. multichannel SAR system [16].

Taking into account technological and cost restrictions, most of the operational and near-future spaceborne SAR-GMTI system are limited to two receive chains. Today's satellites are equipped with programmable antenna arrays that give great operational flexibility. The core of this thesis is the Dual Receive Antenna (DRA) mode of operation, used in TerraSAR-X [13], RADARSAT-2 [8] or COSMO-Skymed [18]. Others antenna configurations are considered, as described in section 3.7.

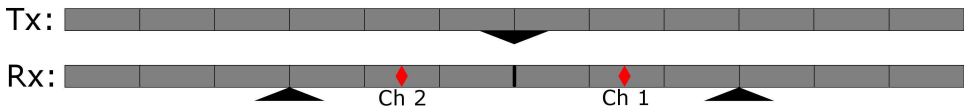

Figure 3.1: Dual Receive Antenna configuration, in transmission the full antenna is used, in reception the antenna is split in two halves. Black triangles indicate the physical centers of the Tx or Rx antennas, red diamonds refer to the two-way phase centers for each channel.

In the DRA mode the transmission of the signal employs the full aperture of the antenna, but the reception is carried out, at the same time, by two half partitions of the antenna array in the along-track direction, see figure 3.1. The signals of both receiving antennas are demodulated, sampled and recorded separately.

3.4 Moving target signal model

In order to understand how GMTI techniques operate the signal model for a moving target is mathematically formulated. Here it is considered an extension of the range equation, seen in section 1.4 of chapter 1.

Considering a flat-earth model and a geometry as depicted in figure 3.2, the range history between the SAR and a moving target on the Earth's surface can be modeled as:

$$R(t) = \sqrt{\left[x_0 + (v_{x0} - v_s)t + a_{x0}\frac{t^2}{2}\right]^2 + \left[y_0 + v_{y0}t + a_{y0}\frac{t^2}{2}\right]^2 + h^2}\ , \quad (3.2)$$

where v and a are target velocity and acceleration, the along-track position is indicated by x and the across-track by y. Values at t=0 are denoted by subscript "0" and h is the altitude of the spaceborne SAR. The satellite speed is v_s and t is the azimuth slow time.

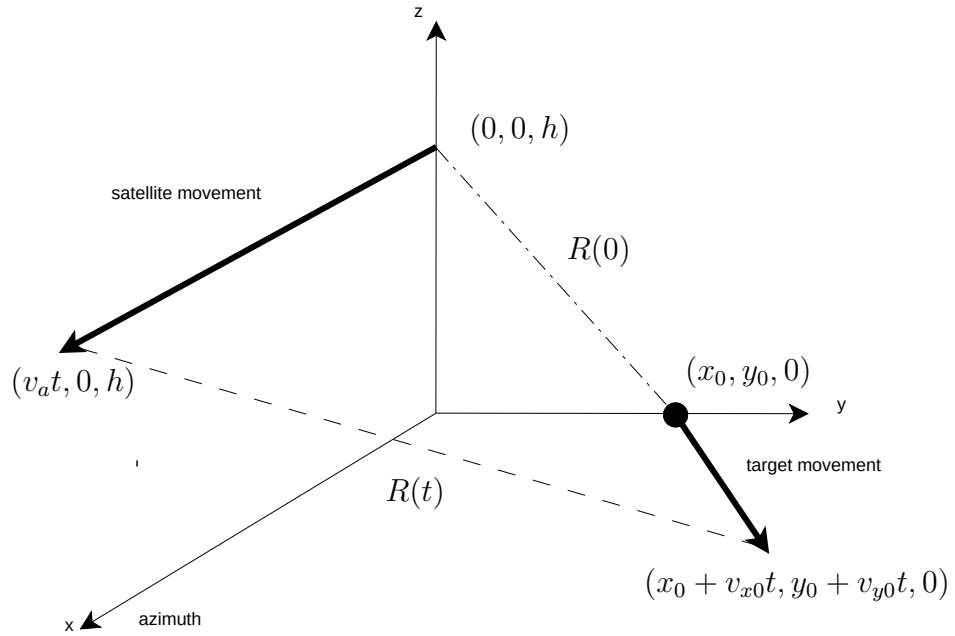

Figure 3.2: A ship moving with constant velocity in a flat-earth geometry with components in the x and y direction. The satellite's flight is in the positive direction x of azimuth. The range history is indicated by $R(t)$.

The target velocity (v_{xb}, v_{yb}) when the azimuth positions of radar coincides with that of the moving target, namely at broadside time t_b, is

$$\begin{aligned} v_{xb} &= v_{x0} + a_{x0}t_b \\ v_{yb} &= v_{y0} + a_{y0}t_b\ , \end{aligned} \quad (3.3)$$

and the broadside position (x_b, y_b) is

$$x_b = x_0 + v_{x0}t_b + a_{x0}\frac{t_b^2}{2} \quad (3.4)$$

$$y_b = y_0 + v_{y0}t_b + a_{y0}\frac{t_b^2}{2} .$$

Hereafter is investigated the signal model for a constant velocity target, i.e. all the acceleration component in the above equation are discarded and hence $v_{xb} = v_{x0} = v_x$ and $v_{yb} = v_{y0} = v_y$. The study of the acceleration effects on SAR-GMTI detection is beyond the scope of the thesis, the reader could refer to [19].

As suggested in [14] equation (3.2) can be approximated by the second-order Taylor expansion around broadside time t_b, that is

$$\begin{aligned} R(t) &\cong R(t_b) + R'(t_b)(t - t_b) + R''(t_b)\frac{(t - t_b)^2}{2} \\ &= R_b + v_y\gamma(t - t_b) + \frac{v_{rel}^2}{2R_b}(t - t_b)^2 , \end{aligned} \tag{3.5}$$

where R_b is the slant range at broadside

$$R_b = \sqrt{y_b^2 + h^2} , \tag{3.6}$$

and

$$\gamma = \frac{y_b}{R_b} \tag{3.7}$$

$$v_{rel}^2 = (v_x - v_s)^2 + v_y^2(1 - \gamma^2). \tag{3.8}$$

Simplifying the equation of the baseband signal (2.7) in chapter 2 and considering a range compression via matched filtering, the received signal from a moving target is given by

$$s(t) = B \exp\left[-j\frac{4\pi}{\lambda}R(t)\right] rect\left(\frac{t}{T_e}\right) , \tag{3.9}$$

where B is a complex amplitude that accounts for the antenna pattern, the reflectivity of the scatterer and the pattern of the antenna, $R(t)$ is the range history between the SAR and a moving target found in (3.2) and T_e is the target exposure time defined in section 1.1.

3.4.1 DRA case

Generalizing the former equation (3.9) for the dual receive antenna mode, the received signals from the two parts of the antenna are

$$\begin{aligned} s_1(t) &= B \exp\left[-j\frac{4\pi}{\lambda}R(t)\right] rect\left(\frac{t}{T_e}\right) \\ s_2(t) &= B \exp\left[-j\frac{4\pi}{\lambda}R(t)\right] \exp\left[-j\frac{2\pi}{\lambda}u(t)d\right] rect\left(\frac{t}{T_e}\right) , \end{aligned} \tag{3.10}$$

where d is the distance between the two receive sub apertures and $u(t)$ is the directional cosine approximated by [14]

$$u(t) = cos(\alpha(t)) \simeq \frac{v_x - v_s}{R_b}(t - t_b) \ , \tag{3.11}$$

where $\alpha(t)$ is the angle between the antenna-target line of sight and the azimuth direction, see figure 3.3. The distance from the target to the SAR is considered large enough such that in the above formula was possible to apply the far-field approximation (echo signals wavefront arrive parallel in the two sub-apertures).

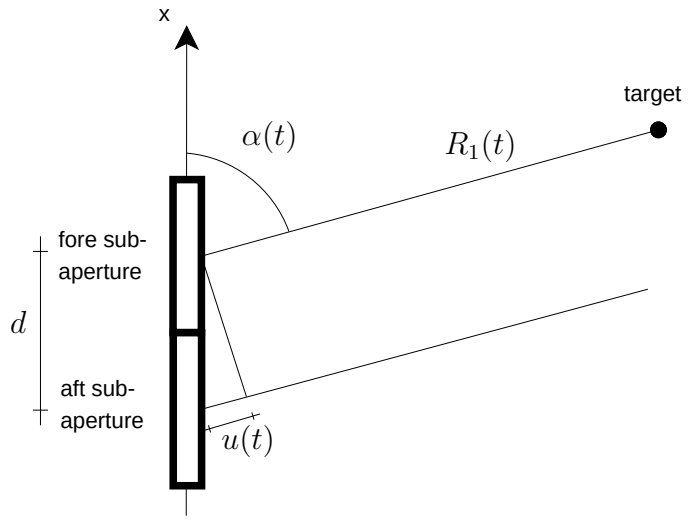

Figure 3.3: Top-down view of satellite antenna and target. In the figure are depicted the distance d between the two antenna sub-apertures in the DRA mode, the angle $\alpha(t)$ between the antenna-target line of sight; $u(t) = cos(\alpha(t))$ refers to the directional cosine.

3.5 Displaced Phase Center Antenna (DPCA)

The Displaced Phase Center Antenna (DPCA) is a simple and common method for clutter suppression for SAR moving target indication [16].

In classical ground-base radars, a stationary background produces identical echoes in successive received signals since neither the antenna nor the clutter moves between pulses. In such a situation, the clutter can be rejected subtracting consecutive received signals, the only energy that remains is due

to moving target or noise. The DPCA is an attempt to apply this principles of clutter suppression to synthetic aperture radars. In addition to the DPCA exist other methods for clutter suppression, for example Space-Time Adaptive Processing (STAP) [27], however are not covered in this thesis.

DPCA requires the use of two antennas displaced along the radar satellite's flight path. DPCA, theoretically, imposes the value of the PRF, that has to be adjusted according to the satellite velocity and the separation of the two antennas (or the two sub-apertures). The DPCA condition stated that the two antennas have to occupy the same spatial position but at different instant of time, see picture 3.4).

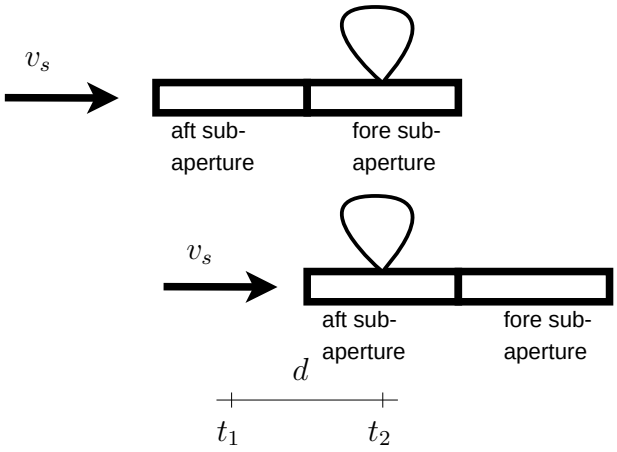

Figure 3.4: Classical DPCA: the phase centers of the fore and aft receive channels coincide in successive time instant t_1 and t_2. Note that the pulse repetition frequency have to be fixed by the satellite speed v_s and antenna distance d.

Basically, DPCA is the difference of complex SAR data from two channels. Stationary objects, i.e. clutter, appear at the same position and hence are canceled by a difference of the complex values images, on the contrary, the echoes by moving targets are preserved. It is possible to demonstrate the restrictions on the PRF could be overcome as it is shown in [26]. It is only required to time shifting one signal by reseampling it, this operation is referred as 'channels co-registration'. With an ideal radar, without noise and with a perfectly stationary clutter, ground sea clutter (and static targets) is completely removed after a DPCA processing. However, for real system, clutter suppression is mainly limited by the noise floor of the radar (as it seen in simulation on chapter 5), co-registration errors and amplitude or phase imbalance of the receive channels [19].

3.5.1 DPCA mathematical expression

It is useful to see the DPCA mathematical expression in order to understand the notch-like filtering performed by DPCA around zero velocity. Resuming the equations (3.10) of the received signals $s_1(t)$ and $s_2(t)$ from the two parts of the antenna in the DRA mode and considering the co-registration of the channels by a time shift of $\frac{d}{2v_s}$, the DPCA output is given by the difference between these two co-registered channels [1]

$$\begin{aligned} DPCA(t) &= s_1(t) - s_2\left(t + \frac{d}{2v_s}\right) && (3.12)\\ &= Be^{-j\frac{4\pi}{\lambda}R(t)}\left(1 - e^{-j\frac{2\pi}{\lambda}E(t)}\right) && (3.13)\\ &= Be^{-j\frac{4\pi}{\lambda}R(t)}e^{-j\frac{\frac{2\pi}{\lambda}E(t)}{2}}\left(e^{j\frac{\frac{2\pi}{\lambda}E(t)}{2}} - e^{-j\frac{\frac{2\pi}{\lambda}E(t)}{2}}\right) && (3.14)\\ &= Be^{-j\frac{4\pi}{\lambda}R(t)}e^{-j\frac{\frac{2\pi}{\lambda}E(t)}{2}}2j\sin\left(\frac{\pi E(t)}{\lambda}\right) , && (3.15) \end{aligned}$$

where B accounts for target reflectivity, transmitted power, antenna pattern and propagation loss and it is possible to consider an approximation for $E(t)$ equal to

$$E(t) = 2R\left(t + \frac{d}{2v_s}\right) + u\left(t + \frac{d}{2v_s}\right)d - 2R(t) \cong \frac{v_y y_b d}{R_b v_s}. \quad (3.16)$$

For some details about E and co-registration refer to [14].

The detection of the moving targets is based on the magnitude of the DCPA, given by

$$|DPCA(t)| \cong 2|B|\left|\sin\left(\frac{\pi}{\lambda}\frac{v_y y_b d}{R_b v_s}\right)\right| , \quad (3.17)$$

where the approximation on equation (3.16) was used. Please note that the argument of the sine is a function of only the across-track velocity v_y and is not dependent upon time t.

In the figure 3.5 is plotted the typical curve of DPCA output amplitude as a function of across-velocity v_y.

From figure 3.5, the notch-like filtering DPCA pattern can be recognized arround the zero velocity

[1] Please note that d is the physical separation of the antennas centers, $\frac{d}{2}$ is the distance between the two-ways phase centers.

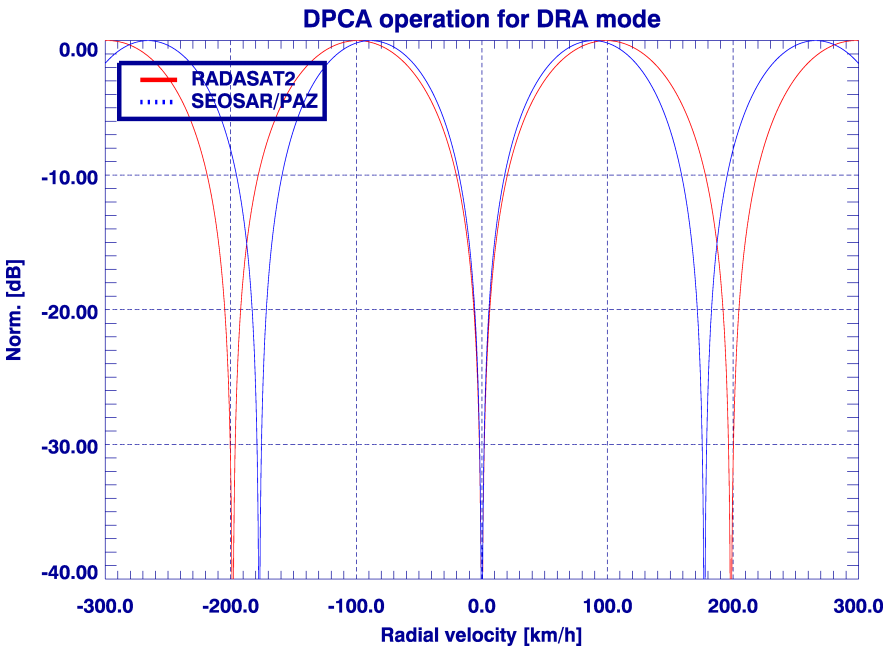

Figure 3.5: DPCA normalized magnitude output for RADARSAT-2 or SEOSAR/PAZ parameters as a function of across-velocity v_y.

Additional notches (ambiguous notches) appear also at non-zero radial velocity due to array spatial sampling and are called blind velocities. It must be noted that a target that possesses zero across-track velocity and only along-track velocity component will be very attenuated at the DPCA output.

3.6 Along-track Interferometry (ATI)

Along-track interferometry (ATI) is another multi-aperture technique used for SAR moving target indication. As for the DPCA case, ATI requires multiple antennas displaced in the along-track direction, in such a way the antennas observe the same scene at different times.

Considering a two-channel SAR system, exploiting for example the DRA mode of operation described in section 3.3, the ATI signal is computed by multiplying the signal from one channel by the complex conjugate of the other channel, that is

$$ATI(t) \quad = \quad s_1(t)s_2^*(t) \tag{3.18}$$

$$= |s_1(t)||s_2(t)|e^{j[\phi_1(t)-\phi_2(t)]} ,$$

where the signals $s_1(t)$ and $s_2(t)$ are here considered already co-registered, the symbol * denotes complex conjugation and $\phi_1(t)$ and $\phi_2(t)$ are the phases of the two received signals.

Differently from the DPCA, in the ATI processing there is no a real cancelation of the clutter. In the ideal case, without noise, a stationary clutter or a still target have zero phase since the two signal phases $\phi_1(t)$ and $\phi_2(t)$ are identical and cancel each other out. A moving target has a non-zero phase related to its movement. Therefore, it is possible to exploit the ATI phase and amplitude to detect moving targets, while the ATI phase of the detected targets provides an estimation of the across-track velocity as will be seen on chapter 4.

ATI phase is subjected to several ambiguities which affect target detection and velocity estimation. For example blind-velocities occur when the slant range variation of the moving target within the two channels is several times the operational wavelength, in a way that the ATI phase is out of the range $\pm\pi$. In addition, Doppler ambiguities are induced due to finite azimuth bandwidth of the system. It is possible to find more information about ATI ambiguities in Appendix B of [19]. However, in a typical case of a ship-sea scenario observed by a spaceborne SAR these ambiguities are not noticeable.

3.7 Beyond two channels: antenna toggle modes

Current implementations of SAR missions, for example TerraSar-X [13] and Radarsat-2 [8], or the future Spanish mission SEOSAR/PAZ [7], have limited GMTI capabilities, operating with just two receivers collocated in along-track direction. As said before, it' s possible to use this two channels via the dual antenna receive mode of operation to cancel clutter using DPCA or to estimate target's parameters using the ATI phase. As was pointed out, the ATI doesn't actually cancel clutter like DPCA, and so the estimation of the target's velocity suffer of clutter contamination.

A way to obtain a better parameters estimation could be to perform an ATI processing after a clutter suppression (DPCA); but using only data from two channels this is impossible: it is required at least an additional channel, see figure 3.6.

In current and near-future satellite mission there is a limit of two physical receiver chains due to cost and technological restriction. Additional virtual channels could be achieved keeping the same system complexity thanks to a clever programming of the phased array antennas. The operational modes using virtual channels are called toggle modes.

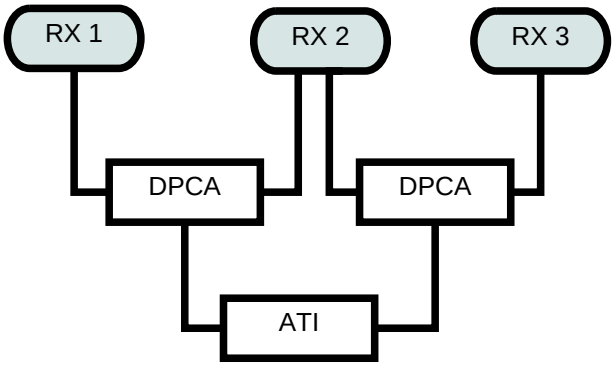

Figure 3.6: ATI performed in two clutter-suppressed images obtained after DPCA processing: are need at least three channels.

In the UPC SAR-GMTI simulator are contemplated toggle receiving modes , where three or four virtual channels are created by special receiver excitation schemes, based on a dual receivers antenna.

This toggling mode is an experimental mode considered in the RADARSAT-2 [11]. In this thesis are just consider two of the different toggling/swithcing modes proposed in [11].

The period of the pulses, in toggle modes, is set to two, i.e. transmission and receive schemes repeats every two pulses. The pulses are transmitted exploiting the full antenna aperture and the echoes are received using two alternating receiver excitation schemes. Note that in the case of toggle modes to compensate clutter band aliasing the PRF have to be doubled

3.7.1 Three virtual channels

In figure 3.7 it is shown a possible way to realize a three virtual channel on receive system: for odd pulses the transmission is done with the whole antenna and the backscattered signal is received with the two sub-apertures obtained splitting up the whole antenna in two equal parts (as in the DRA case); at even pulses the signal is transmitted with the whole antenna and the backscattered signal is received with a single centered sub-aperture having the same length of the first two.

3.7.2 Four virtual channels

In figure 3.8 it is shown a possible way to realize a four virtual channel toggle on receive system: for odd pulses the transmission is done with the whole

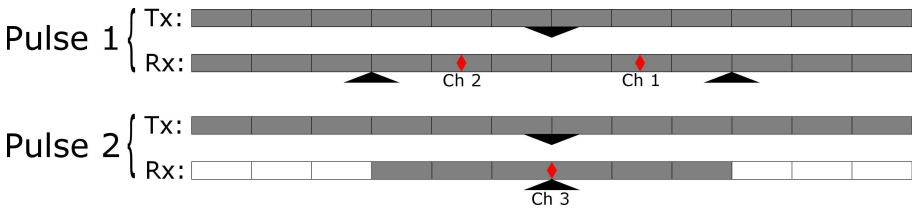

Figure 3.7: Three virtual channel toggle on receive configuration of the antenna for the two subsequent pulses, black triangles indicate the physical centers of the Tx or Rx antennas, red diamonds indicate the two-way phase centers for each virtual channel.

antenna and the backscattered signal is received with two sub-apertures obtained splitting up the whole antenna in four equal parts and using only two of that; at even pulses the signal is transmitted with the whole antenna and the backscattered signal is received with the two remaining sub-apertures.

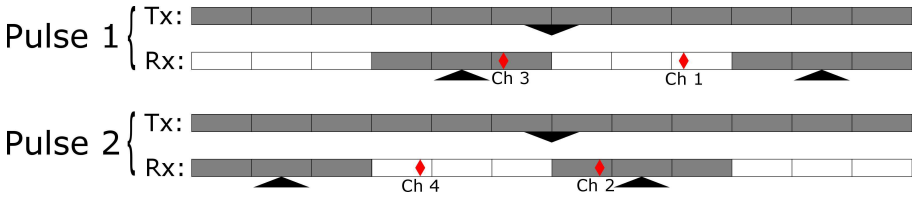

Figure 3.8: Four virtual channel toggle on receive configuration of the antenna for subsequent pulses, black triangles indicate the physical centers of the Tx or Rx antennas, red diamonds indicate the two-way phase centers for each virtual channel.

3.7.3 Considerations on toggle modes

Some considerations have to be done for these toggle modes of operation. For the toggle modes already present, where the excitations of the antenna on receive are varied from pulse to pulse, the operational pulse repetition frequency PRF should be doubled in order to avoid ambiguities . This fact implies that to keep a power consumption similar to the DRA mode the energy-per-pulse have to be reduced by the same amount the PRF is increased, and so decreased by half. The SCR doesn't change because the energy of the clutter is dependent on the energy of the pulse, but the SNR inevitably decreases.

The third and fourth channels provide new possibilities in the processing stage, as a matter of fact it's possible to perform an ATI of two images where the clutter was canceled by a DPCA. Furthermore, with toggle modes is possible to chose among different lengths of baselines, i.e. length differences between the phase centers, and this has effects on the performance of the DPCA and ATI, as shown in the simulations in chapter 5.

In general, it is possible to consider also a four channels toggle *transmit* mode [11] where pulses are transmitted from different halves of the antenna between consecutive pulses. The echoes are received using two sub-apertures of the full antenna (as in the DRA mode). Similarly to the other toggle modes some preliminary considerations have to be done. As in the other modes the PRF should be twice due to the odd and even pulses, but as the effective TX antenna in the toggle transmit mode is half, the PRF in conclusion should be quadrupled in order to correctly sample the Doppler bandwidth according to the Nyquist criteria. This is obviously a very hard request for the actual satellite systems and almost impossible because of the upper limit on the PRF value present in such SAR radars. In this thesis and using the UPC-SAR simulator with SEOSAR/PAZ like parameters this mode of operation has not been considered.

Chapter 4

Detection and estimation

In the previous chapter, state-of-the-art GMTI techniques with synthetic aperture radars were delineated: Displaced Phase Center Antenna (DPCA) for clutter suppression and Along-track Interferometry (ATI).

The first part of this chapter illustrates the use of these methods to implement a DPCA Constant False Alarm Rate detector and a across-track velocity component estimation by ATI. Furthermore, it is briefly explained the utility of the Fractional Fourier Transform (FrFT) to estimate the along-track velocity component of a moving target. In the second part of the chapter the proposed detection and estimation schemes are described in detail to be further integrated as a module in the UPC-SAR-GMTI simulator tool.

4.1 Moving target detection

Target detection requires an automatic system that decides over all the points, for example in the focused images, which are moving objects.

The probability of detecting a moving target is maximized subject to the constraint that the false alarm probability [1] does not exceed a specified level. In this sense a threshold is statistically characterized by the Probability Density Function (PDF) of the signal in the domain where the detection is performed, e.g. the magnitude of the signal at the output of the DPCA.

If this threshold is too low, the probability of detection will increase, for given conditions, at the expense of increased number of false alarms. And, the other way around, when the threshold is too high then fewer targets will

[1] The probability of false alarm P_{FA} is the probability deciding that there is a moving target when, actually, it is not present.

be detected, but the number of false alarms will also be low. In the radar's framework it is preferred to design detectors where a required probability of false alarm is fixed; this detectors are called as Constant False Alarm Rate (CFAR) [28].

4.1.1 Constant False Alarm Rate DPCA detector

After processing the channels via DPCA (see section 3.5),under ideal operation, i.e. clutter is perfectly canceled, the output of the DPCA is modeled as a complex Gaussian distribution

$$f_{I_D}(I_D) = \frac{1}{2\pi\sigma_D^2} e^{-\frac{1}{2\sigma_D^2}[\Re(I_D)]^2+[\Im(I_D)]^2} , \tag{4.1}$$

where I_D is the DPCA output, σ_D^2 is the variance of the real and imaginary parts (supposed uncorrelated) and $\Re()$ and $\Im()$ refer to real and imaginary parts, respectively.

The input of the Constant False Alarm Rate DPCA detector is the magnitude of the DPCA signal, $A = |DPCA|$, which is characterized by a Rayleigh distribution because is the absolute value of a complex Gaussian distributed signal

$$f_{|A|}(A) = \frac{A}{\sigma_D^2} e^{-\frac{1}{2\sigma_D^2}A^2}, \quad A \geq 0 . \tag{4.2}$$

The magnitude of DPCA has to be compared against a threshold η_{th}, see figure 4.1, which has been calculated according to a specific probability of false alarm as

$$P_{FA} = \int_{\eta_{th}}^{\infty} f_{|A|}(A) dA . \tag{4.3}$$

Although is not implemented in this thesis the output ATI signal could be compared with a specific threshold to form ATI CFAR detectors, in a similar way as for the DPCA. Exists three possible approaches of CFAR detection with ATI [29].

A non optimal but simple solution is to consider only the information of ATI phase, it is referred as one-step ATI CFAR detector. The phase information of a moving target is related with its movement and different from zero, as it is the ideal case of perfectly stationary clutter, see section 3.6. A two-step ATI CFAR detector can be implemented when considering also the ATI magnitude. In this case, the phase and magnitude are assumed independent, and two different thresholds are specified separately for the phase and magnitude based on the marginal density probability functions.

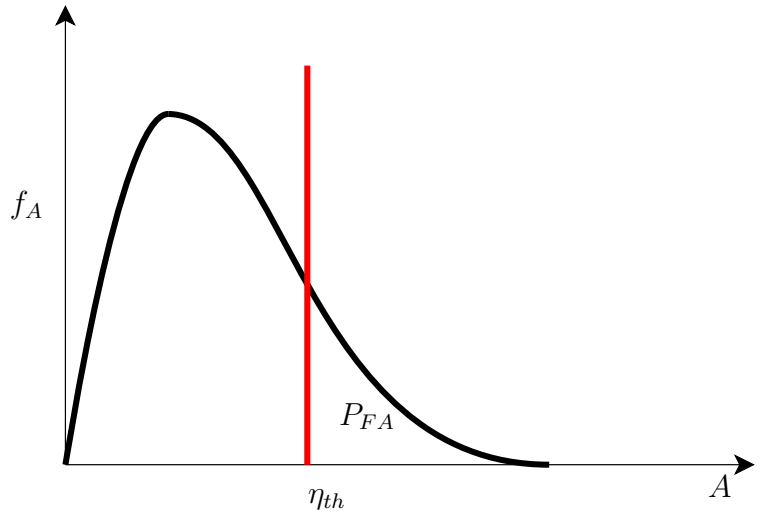

Figure 4.1: Magnitude of the outupt DPCA signal characterized by a Rayleight distribution. Threshold η_{th} and probability of false alarm P_{FA} are depicted.

However, in order to include the coupling between the magnitude and phase, exploiting all the information retrieved by ATI, is necessary to build a two-dimensional ATI detector. In this case, the threshold is calculated based on the joint probability density function, see [30].

4.2 Moving target velocity estimation

This section describes the estimation procedures to retrieve the along-track (azimuth) and across-track components of the moving target's velocity vector. It is important to point out that the across-track velocity induces an azimuth Doppler shift in the signal, whereas, the along-track component impacts on the azimuth FM rate K_a, see (2.13), called also Doppler slope.

Generally, the SAR processor assumes a stationary scene and therefore employs a Stationary World Matched Filter (SWMF) to compress in azimuth direction, focusing the targets at their zero-Doppler position. As a consequence of the Doppler shift, the moving targets with non-zero across-

track velocity component, appear focused in a shifted azimuth position, see figure 4.2. In the case of targets with non-zero along-track velocity component, they appear defocused and smeared due to the mismatch respect to the SWMF in terms of Doppler rate or slope, see figure 4.3. The estimation of the targets' velocity vector provides a way to correct displacement and defocusing.

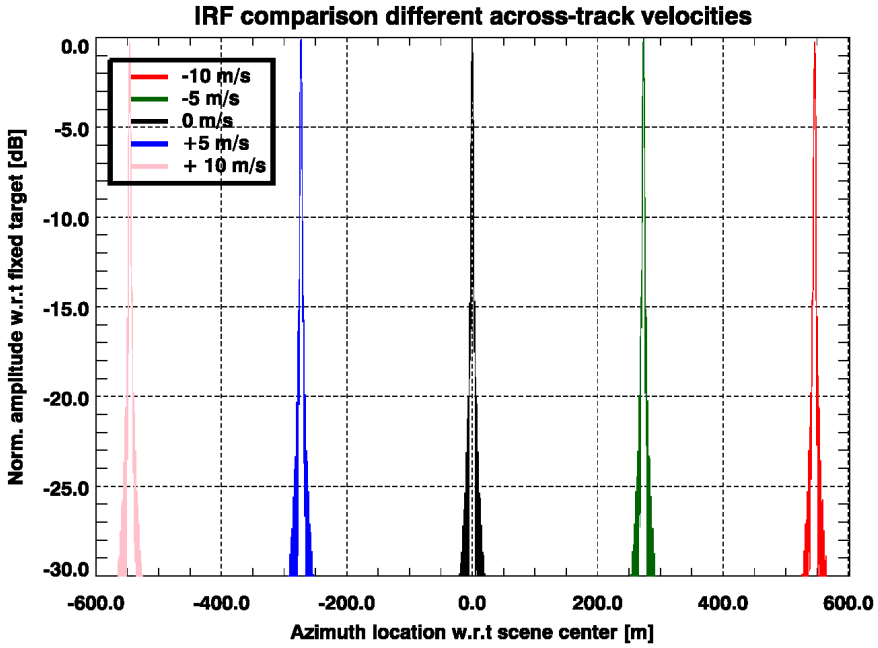

Figure 4.2: Azimuth cut of the impulse response function of a moving target with different constant across-track velocities. The target will be focused in different azimuth position [31].

4.2.1 Across-track velocity component estimation

To obtain an estimation of the across-track velocity the interferometric phase is exploited. Considering a stationary world matched filter, a zero-acceleration moving target and applying the ATI equation (3.18), the ATI phase follows this relation [19]

$$\angle ATI = \frac{2\pi}{\lambda}\frac{1}{2R_0}dy_0 v_{across}\left(\frac{1}{v_s} - \frac{v_{along}-v_s}{(v_{along}-v_s)^2 + v_{across}^2(1-\frac{y_0^2}{R_0^2})}\right) , \quad (4.4)$$

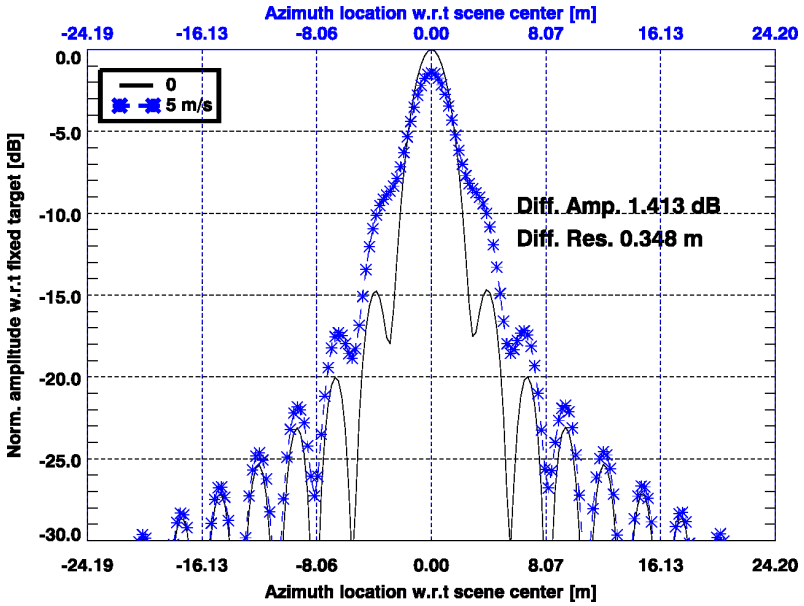

Figure 4.3: Impulse response function analysis (azimuth cut) of a moving target with different constant along-track velocity against a fixed target [31].

where λ is the wavelength, d the distance between antenna phase centers, R_0 and y_0 the range of closest approach and distance target-nadir, respectively, and the satellite velocity is indicated by v_s. Often the ATI phase is approximated by [32]

$$\angle ATI \simeq \frac{2\pi}{\lambda 2 R_0 v_s} dy_0 v_{across} \ , \tag{4.5}$$

which stands for the SAR spaceborne case as indicated in [2], and therefore it is used throughout all this thesis.

In this way, the across-track velocity $v_y = v_{across}$ is directly proportional to the ATI phase and it is computed as

$$v_{across} = \frac{R_0 v_s}{\frac{2\pi}{\lambda} dy_0} \angle ATI \ . \tag{4.6}$$

4.2.2 Along-track velocity component estimation

A classical way to estimate the along-track velocity component is by means of a bank of matched filters, [19]. These filters are used in replacement of the stationary world matched filter (SWMF). This technique compresses the

signal with different filters (matched to different along-track velocities) and try to maximize the response of the target in the final image.

In the UPC-SAR simulator it was experienced that this bank of matched filters' technique gives really poor along-track velocity estimation, with errors up to 10 m/s [33]. This occurs for the reason that the output of the bank is almost the same for the different velocities in the spaceborne case as a consequence of considering really small along-track velocities compared to the satellite velocity.

In this thesis an alternative way to estimate the along-track velocity is analyzed. In place of a bank of filters procedure, a relatively unknown powerful technique is used, as suggested in [34]: the Fractional Fourier transform (FrFT). The mathematical details about this transformation could be found in [35]. Fractional Fourier is a generalization of the classical Fourier transform where a signal is transformed in a hybrid time-frequency domain. The FrFT depends on a parameter α and can be interpreted as a rotation by an angle α in the time-frequency domain. As shown in section 2.1the SAR signal, both of a fixed or moving target, is nearly a linear chirp in the azimuth slow time domain. Exploiting this property, each target (fixed or moving) is characterized by a given rotational angle, and can be accordingly focused in an optimum Fractional domain, see figure 4.4.

It should be noted that the use of FrFT is performed in range compressed but azimuth uncompressed SAR data. The SAR-GMTI techniques, such as DPCA and ATI, can be carry also in the these azimuth uncompress data. The limited SNR of an uncompressed azimuth data is compensated by the capability of FrFT of concentrated the moving target energy in few samples in the optimum Fractional domain, improving the SNR. Differently from standard techniques with the Fractional Fourier transform a better along-track velocity estimation is reached, as shown in the simulation results in chapter 5.

The optimum fractional rotation angle α for a specific target is directly related to its Doppler slope, or azimuth FM rate, K_a, defined in (2.13) and it is given by [36]

$$\alpha = \arctan\left(-\frac{PRF^2}{K_a N}\right) , \tag{4.7}$$

where PRF is the pulse repetition frequency used in the satellite and N the number of samples of the signal analyzed.

Finally, the along-track velocity $v_x = v_{along}$ is estimated from the rotation

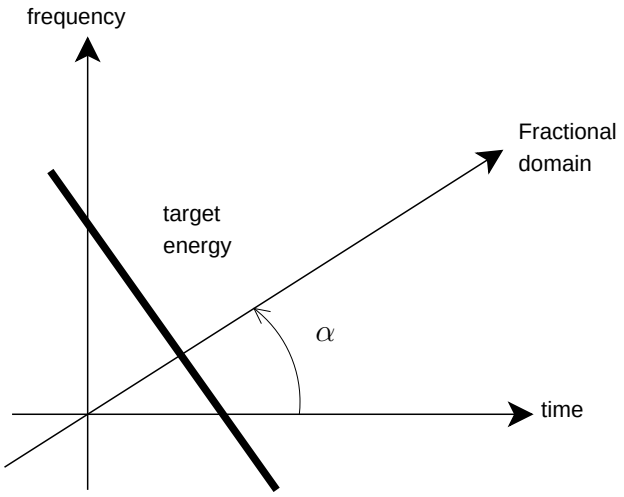

Figure 4.4: Illustration of the Fractional Fourier transform domain, α is the rotational angle of the FrFT. A moving target energy information is also depicted.

angle α by [34]

$$v_{along} = v_s - \sqrt{\frac{R_0 \lambda PRF^2 \cot \alpha}{2N} - v_{across}^2 \left(1 - \frac{y_0^2}{R_0}\right)}\,, \tag{4.8}$$

where R_0 and y_0 are the range of closest approach and the distance target-nadir, respectively. Note that v_{along} depends also from the across-track velocity v_{across}, which hence has to be estimated first.

4.3 Detection and estimation algorithm

In figure 4.5 a flowchart of the proposed algorithm for moving targets detection and velocity estimation for the two channels DRA mode is shown.

The channels have to be co-registered before DPCA; this operation is performed as an interpolation by a linear phase operation in the frequency domain. Co-registered channels are processed by the first two steps of the Range Doppler algorithm described in section 2.2: a range compression and range cell migration correction are carried out. With this range-compressed and co-registered channels a single DPCA image is generated.

In order to preserve all the energy of the moving targets is not applied a stationary matched filter, which could defocused the targets, but the detection is performed over the azimuth uncompressed signals.

Considering the output image from the DPCA, every azimuth line [2] is transformed into the specific Fractional domain. The Fractional domain is, for every azimuth line, the one in which is found a peak of maximum magnitude, varying the rotational angle α. This specific Fractional domain is associated with an optimum rotational angle $\alpha_{opt,i}$. Where subindex i refers to the different range lines. It has been assumed that just a single moving target is considered for each range bin. Therefore the optimum rotational angle $\alpha_{opt,i}$ is found only searching for one maximum peak. Multiple moving targets for azimuth line would mean to search for more than one maximum peak. The peak magnitude value is compared with a threshold for a CFAR detection. The way how is obtained this threshold for the detection in the Fractional domain is explained in the following section.

If the peak magnitude exceeds the threshold means that a moving target is detected. The value of the azimuth line rg_i where is found the moving target, the optimum rotational angle $\alpha_{opt,i}$ and peak position $u_{p,i}$ in the Fractional domain are kept in order to perform the velocity estimation in a latter step.

Once the moving target has been detected its velocity vector can be estimated, first the across-track component and then the along-track one.

The signal before the DPCA, which is range-compressed, azimuth uncompressed and co-registered, for every azimuth line rg_i and for both channels, is directly mapped into the Fractional domain using the optimal rotational angle $\alpha_{opt,i}$ found during detection.

The peaks for both channels will be exactly in the $u_{p,i}$ position but in this case the signals will be still contaminated by clutter and noise, their extraction is performed using single-sample window centered at u_p position

[2] That is a vector of all azimuth samples.

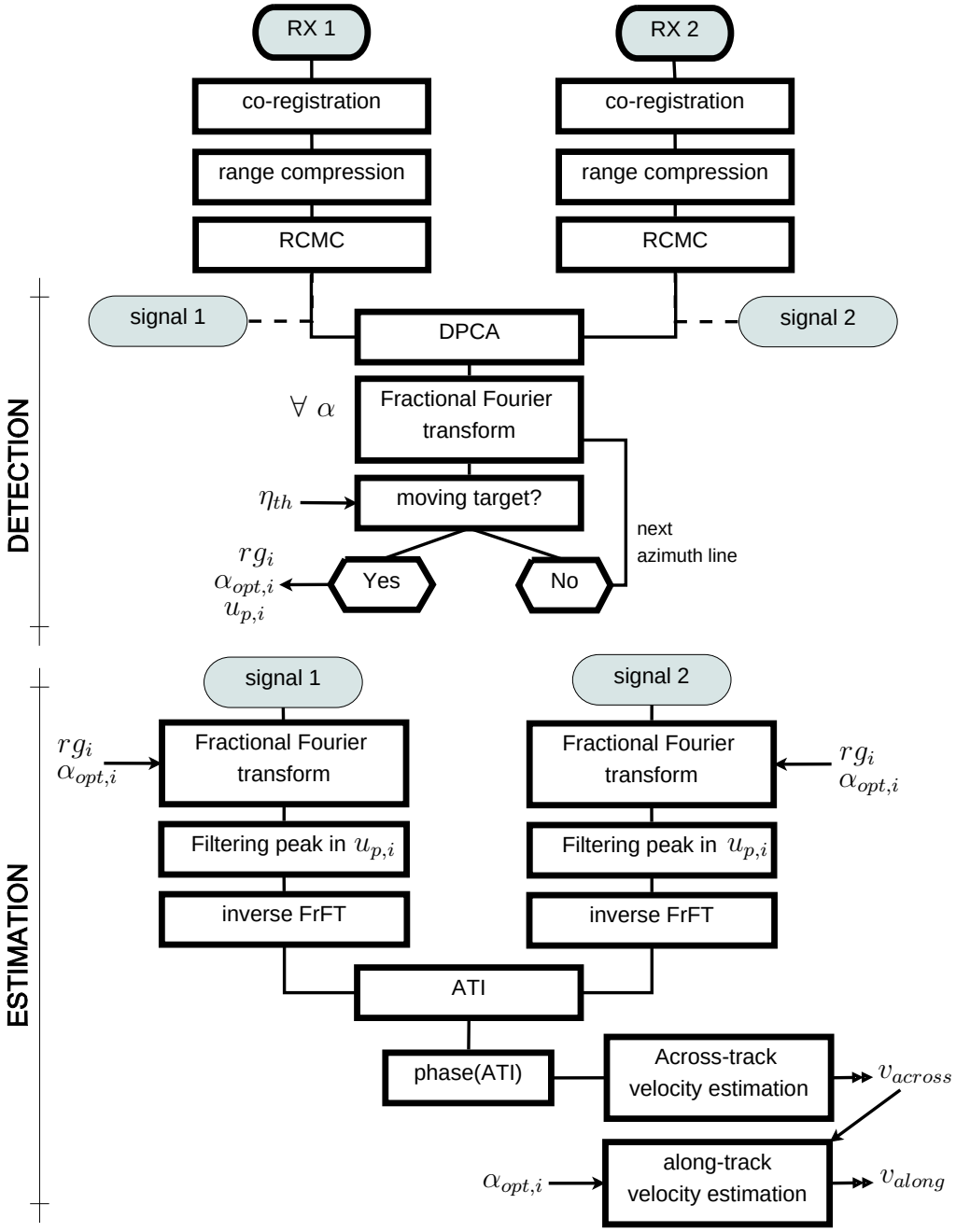

Figure 4.5: Simplified flowchart of the proposed moving target signal detection and velocity estimation algorithm for the dual receive antenna mode.

and zero elsewhere [3]. This filtering leads to clutter suppression and noise reduction, see figure 4.6.

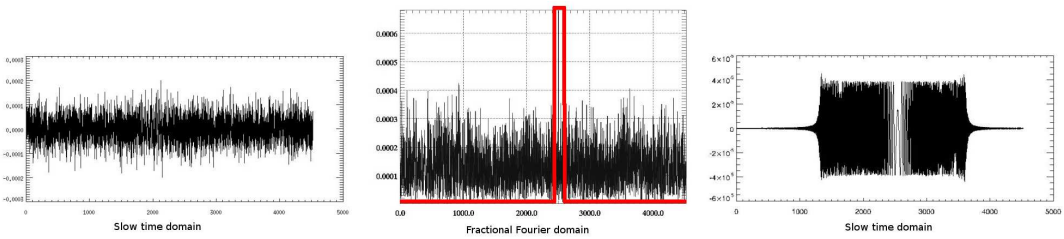

Figure 4.6: Example of bandpass filtering performed in fractional domain for clutter and noise reduction. On the left the original signal in the azimuth slow time domain, in the middle the filtering in the Fractional domain and on the right the signal after an inverse FrFT. Note, in the right, the typical characteristic of a chirp signal (real part).

After an inverse FrFT, an interfergram is formed with these two reconstructed clutter suppressed moving targets filtered signals. From the ATI phase with the formula (4.6) the across-track velocity v_{across} is estimated.

Finally, using v_{across} value, the optimum rotational angle α_{opt} found during detection and with formula (4.8), the along-track velocity is estimated.

Implementation with toggle modes

Figure 4.7 show the algorithm proposed for the toggle modes of operation (see section 3.7) with three or four virtual channels. The procedure is basically the same of the as the previous one. As a consequence of three or four channels available with toggle modes there is no need to return to the range compressed co-registered signals, i.e. before the DPCA, to perform the ATI for parameters' estimation.

[3] This is equal to bandpass filtering. In this case the filter is an ideal rectangular window of only one sample different from zero.

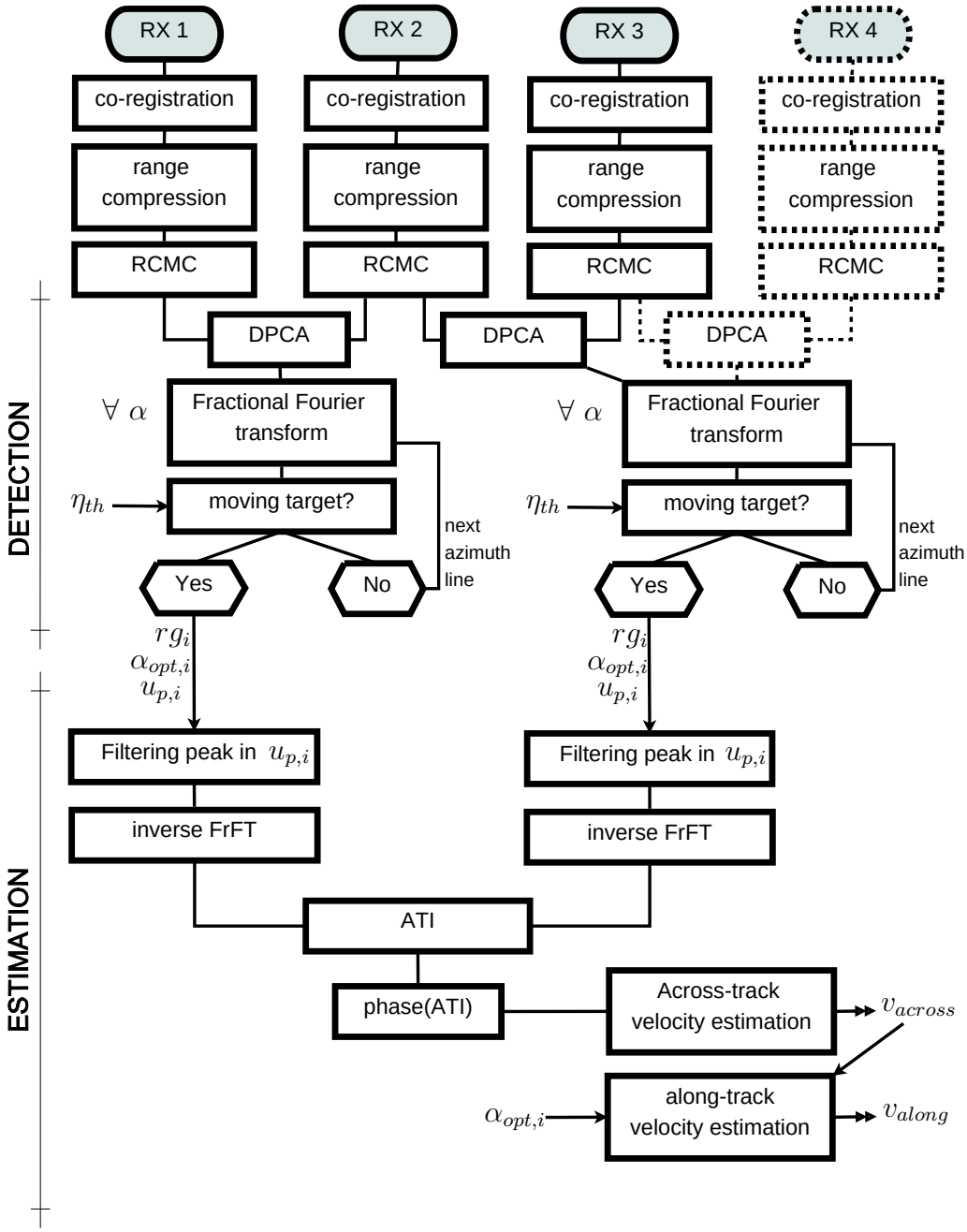

Figure 4.7: Simplified flowchart of the proposed moving target signal detection and velocity estimation algorithm for three or four (dashed part) virtual channels, which can be obtained operating the toggle modes.

4.3.1 Threshold n_{th} calculation

The detection is performed in the Fractional Fourier time-frequency hybrid domain after a DPCA processing. It is supposed that the signal magnitude $A = |s_{FR}|$ after DPCA in the Fractional domain is characterized by a Rayleigh distribution as in the time domain (section 4.1),

$$f_A(A) = \frac{A}{\sigma^2} e^{-\frac{1}{2\sigma^2}A^2}, \quad A \geq 0 \ . \tag{4.9}$$

The estimation of the σ^2 parameter from samples a_i in the Fractional domain could be approximated by [37]

$$\sigma^2 \approx \frac{1}{2N} \sum_{i=1}^{N} a_i^2 \ , \tag{4.10}$$

and the threshold η_{th} could be calculated, according to a specific probability of false alarm, resolving this integration numerically

$$P_{FA} = \int_{\eta_{th}}^{\infty} f_A(A) dA \ . \tag{4.11}$$

It is important to note that this method of estimating the threshold n_{th} can be applied under the condition that there are not many moving targets in the image. To give the reader an idea, an error of 3.7% in the estimation of the σ parameter is obtained considering a sea scene of 1 km $\times$ 1 km, a range and azimuth SAR resolution of $\Delta = 2.5$ m, and a high RCS moving ship of 25 m $\times$ 64 m [33]. A possible solution in case there are too many moving targets in the image is to discard iteratively the higher backscattered samples up to an error estimation of σ lower than 1%, for more details refer to [33].

Chapter 5

Simulation results

The objective of the UPC-SAR-GMTI simulator is to evaluate the applicability and performance of Ground Moving Target Indication techniques applied in spaceborne SAR systems in order to understand their limitations, allowing the proposal of both improved processing techniques as well system architecture/configurations [38]. The proposed techniques, explained in chapter 4, for target detection and velocity estimation were integrated in this UPC simulator tool. This chapter presents simulation results to evaluate the performance of the proposed techniques in terms of Signal-to-Clutter-and-Noise ratio, probability of detection and velocity estimation both for the Dual Antenna Receive and toggle modes.

5.1 General satellite parameters

The SAR system parameters considered in the different simulations, taking as reference the Spanish SEOSAR/PAZ mission, are summarized in table 5.1. It is important to note that in the case of the toggle mode of operation the value for the PRF is doubled and the pulse duration is the half.

5.2 Evaluation of the SCNR

The Signal to Clutter and Noise ratio (SCNR)is evaluated in the fractional domain after the DPCA processing, since the CFAR detection is performed in the hybrid domain. The simulations results shown in figures 5.1 to 5.7 are carried out considering a target with a Radar Cross Section (RCS) fixed to 10 dBsm and for different sea state conditions. In the case of toggle mode of operation the performance of the different available baselines are compared.

Orbit height	510 km
Satellite velocity	7.6 km/s
Radar frequency	9.65 GKz
Antenna dimensions	4.8 m $\times$ 0.7 m
BW of transmitted signal	75 MHz
Sampling frequency	110 MHz
PRF	3.92 KHz
Look angle	39.2 degree
Noise Temperature	790K
Pulse duration	$59\mu s$

Table 5.1: Parameters used for the simulations, they are similar to those of SEOSAR/PAZ satellite.

The parameters used to characterize the clutter in these simulations are with calm, moderate and very rough sea. Table 5.3 indicates the related values of sea state, mean reflectivity coefficient σ_0, temporal decorrelation τ_c and wind speed v_w. These parameters were defined in section 3.2 of chapter 3.

	sea state	v_w	τ_c	σ_0
Calm sea	0	1.5 m/s	60ms	-25 dB
Moderate sea	4	10 m/s	32ms	-15 dB
Very rough sea	6	16 m/s	31ms	-12 dB

Table 5.2: Parameters used for the simulations of different sea clutter.

DRA case

In figure 5.1 the SCNR is represented for a target, which has only *across*-track velocity component, evaluated for the three different sea states. The first thing to note is the notch-like filtering centered in zero velocity. This is directly related to the selectivity for low velocities of the DPCA as was shown in figure 3.5 of chapter 3. Concerning the sea state is observed a difference of $4dB$ from the calm to the very rough condition.

In Figure 5.2 the SCNR is represented as a function of different along-track velocities (keeping across-track component to zero). As expected the values for the SCNR are very low, this in consequence of the use of the

DPCA for clutter suppression. DPCA is sensitive to the radial velocity but the along-track component have minimum impact on it.

The SCNR for a target that moves with the same velocity in both across and along-track direction is reported in the figure 5.3. The trend is practically the same as in the case of a target that moves with only across-track velocity and there is nearly no SCNR loss for high velocities. This is a difference with standard technique using only DPCA where normally high along-track movement caused a defocusing and a consequent signal power loss of the target. In the fractional transform domain this doesn't happen due to the the fact that all the energy of the target is concentred in a single line in the hybrid domain (transformed domain) 4.2.

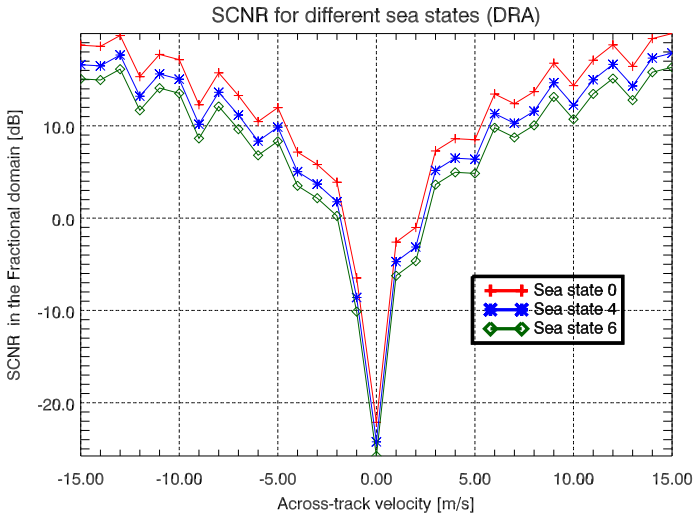

Figure 5.1: SCNR after DPCA in the Fractional Fourier Domain for a target of RCS=10dBsm moving only with *across*-track velocity component for the DRA case. The SCNR is evaluated for different sea states.

Virtual channels toggle antenna modes

Regarding the use of the antenna for creating additional virtual channels seen in section 3.7, in the figures 5.4 and 5.5 are plot the SCNR for a target that moves with the same velocity in both across-track and along-track direction. The SCNR are evaluated for different sea states and for three and four virtual channels, respectively. Note that in figures 5.4, for the three virtual channel and 5.5, for the four virtual channels, the difference on the sea condition practically caused no SCNR variation. This is a clear indication that the

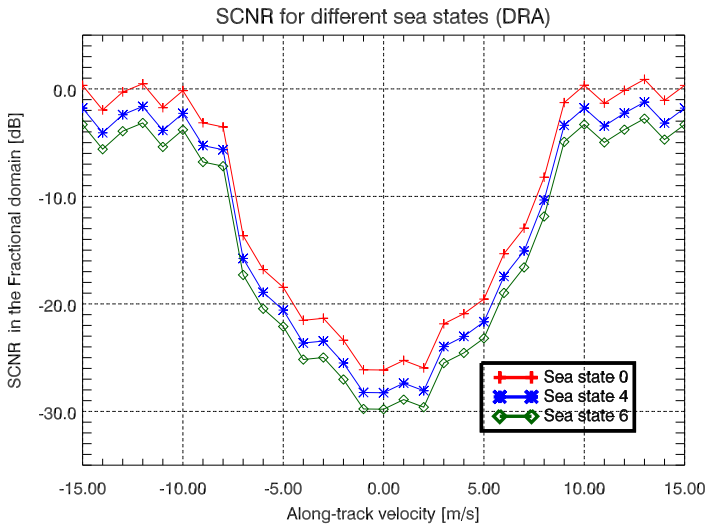

Figure 5.2: SCNR after DPCA in the Fractional Fourier Domain for a target of RCS=10dBsm moving only with *along*-track velocity component for the DRA case.

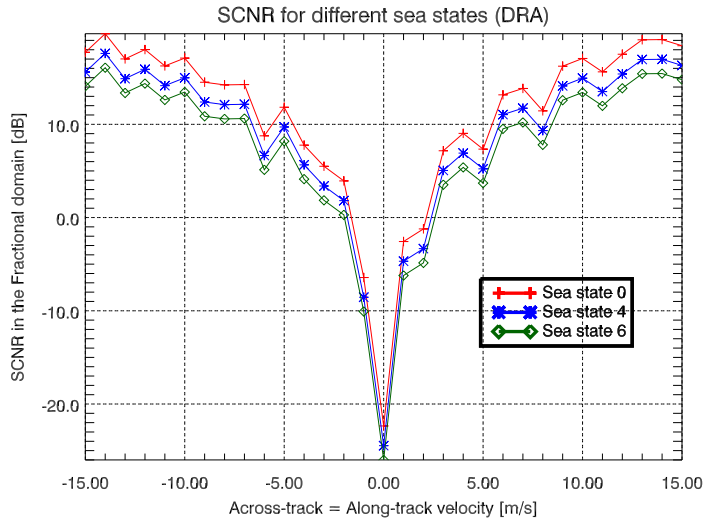

Figure 5.3: SCNR after DPCa in the Fractional Fourier domain for a target of RCS=10dBsm, moving both in the along-track and across-track velocity components for the DRA case.

toggle modes of operation with the parameters utilized in the simulations, are limited by the noise level. In fact, taking into account that there is reduced pulse duration to keep the same energy consumption of DRA case, the gain compression compared to the DRA mode is reduced and so the SCNR.

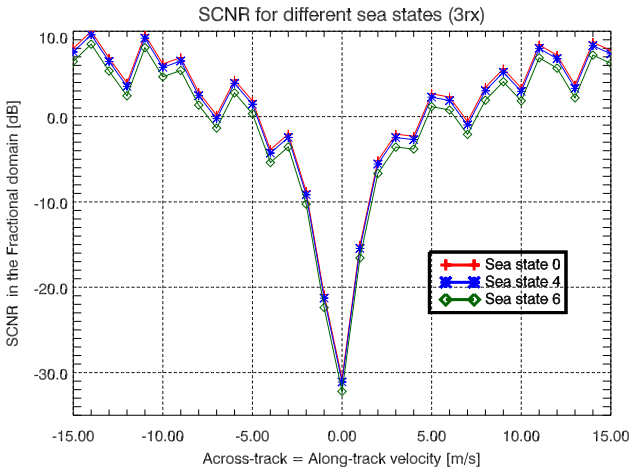

Figure 5.4: SCNR after DPCA in the Fractional Fourier domain for a target of RCS=10dBsm, moving both in the along-track and across-track velocity components for the toggle *three* virtual channels mode of operation. The baseline considered is the one between channel 1 and 2 (look at figure 3.7).

In figures 5.6 and 5.7the SCNR values are reported considering different available baselines for the two toggle modes, respectively. Looking at the figures 3.7 and 3.8 of chapter 3 the baselines considered for the three virtual channel mode are between channel 1 and 2 (equal to 1.2 m) and between channel 1 and 3 (equal to 0.6 m); for the four channel modes are between channel 1 and 4 (equal to 1.8 m), between channel 1 and 3 (equal to 1.2 m) and between channel 1 and 2 (equal to 0.6 m).

Comparing the DRA with the toggle mode there is a general loss in the SCNR value for the virtual channel case. This fact is directly related to the requirement chosen to keep a power consumption similar to the DRA mode, so the energy-per-pulse have to be reduced by half. The SCR doesn't change because the energy of the clutter is dependent on the energy of the pulse, but the SNR inevitably decreases. As a consequence the SCNR also decreased.

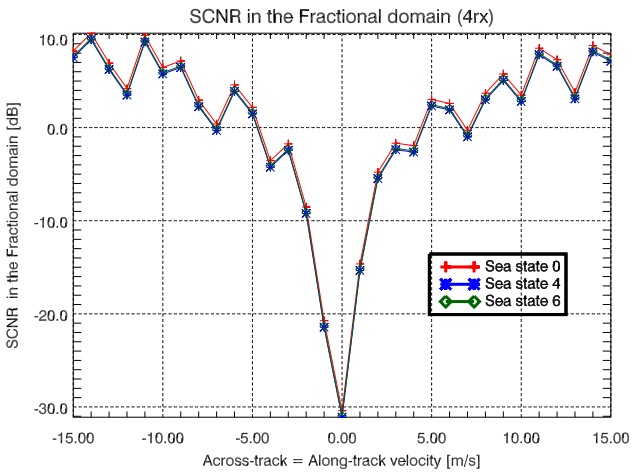

Figure 5.5: SCNR after DPCA in the Fractional Fourier domain for a target of RCS=10dBsm, moving both in the along-track and across-track velocity components for the toggle *four* virtual channels mode of operation. The SCNR is evaluated for different sea states. The baseline considered is the one between channel 1 and 3 (look at figure 3.8).

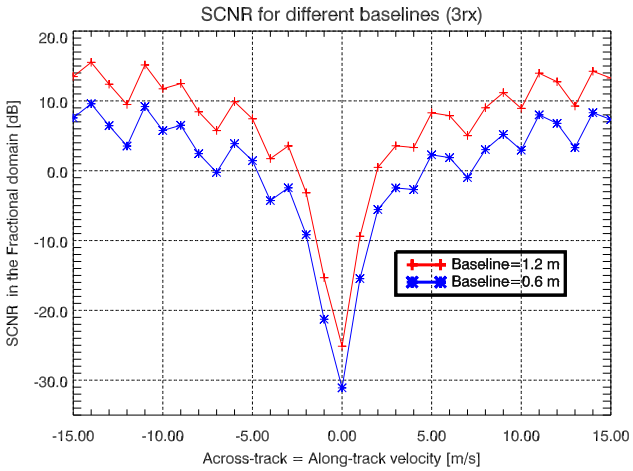

Figure 5.6: SCNR after DPCA in the fractional Fourier domain for a target of RCS=10dBsm, moving both in the along-track and across-track velocity components for the toggle *three* virtual channels mode of operation.

5.3 Probability of detection approximation

To evaluate the probability of detection in different conditions, intense simulations were carried out. The necessity to provide a probability of detection

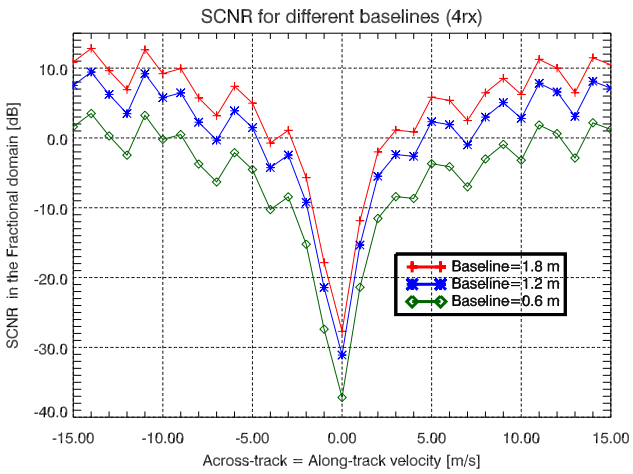

Figure 5.7: SCNR after DPCA in the fractional Fourier domain for a target of RCS=10dBsm, moving both in the along-track and across-track velocity components for the toggle *four* virtual channels mode of operation.

with statistical significance it is accomplished by a sufficient number of samples to asymptotical characterize the random processes involved (clutter and noise). In the following images the rate of detected targets over the total of trials (in this case 30) is represented, this is called the relative frequency of detected a target. It is similar to montecarlo simulations but in this case were generated the whole raw data for different iterations instead of a theoretical approach.

To evaluate the probability of detection just the sea state 4 has been simulated. Moreover, as a consequence of the symmetry of the problem (as showed also by the SCNR images) simulations have been carried out considering just positive velocities (from 1 m/s to 15 m/s).

Four different value of RCS were assumed to model different boats (its response is simplified to a single-point like target):

Boat type	Typical dimension [sm]	RCS value [dBsm]
Motorboat or inflatable boat	3 x 8	0
Small fishing boat	20 x 5	10
Fishing vessel	60 x 10	20
Ferry boat or big vessel	100 x 20	30

Table 5.3: RCS parameter used for the simulations of different type of boats.

Dual Antenna Receive case

The probability of detection for across-track only velocity component is represented in figure 5.8 for the DRA mode for different RCS, ; whereas figure 5.9 shows this metric for a target with equal velocity components. As exoected, in the case of only along-track velocity component the number of target detected was zero for all the trials considered. Therefore for the DPCA case it is impossible to detect a moving target, neither large or small, with only along-track component.

The similarity of the figure 5.8 and 5.9 once again evidence that there is practically the same performance for the only across-track case and for along equal to across-track velocity. Summarizing the results, a target with RCS of 30 dBsm is practically always detected and also a target of RCS 20 dBsm that moves more than 4 m/s. The case of interest is the one of a target of RCS 10 dBsm, which for velocities below 6 m/s is nearly impossible to be detectable. A small boat of RCS 0 dBsm is practically undetectable, also if it moves very rapidly.

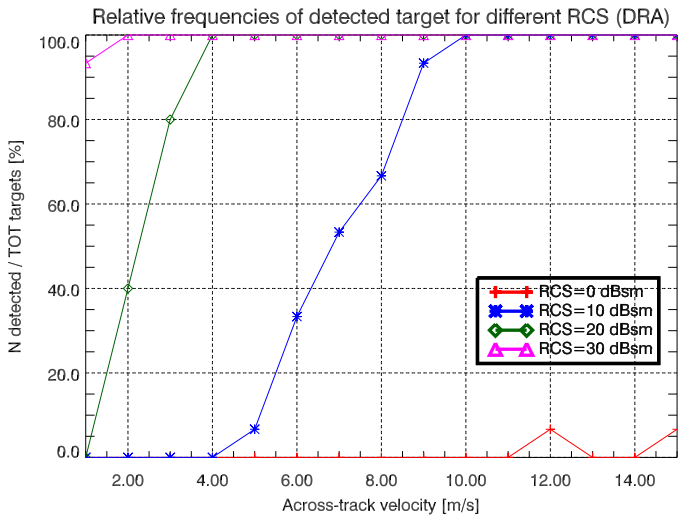

Figure 5.8: Relative frequencies of detected targets moving only with positive *across*-track velocity component for the Dual Antenna Receive mode of operation. The relative frequencies are plotted for different modeled boats, i.e. for different RCS values.

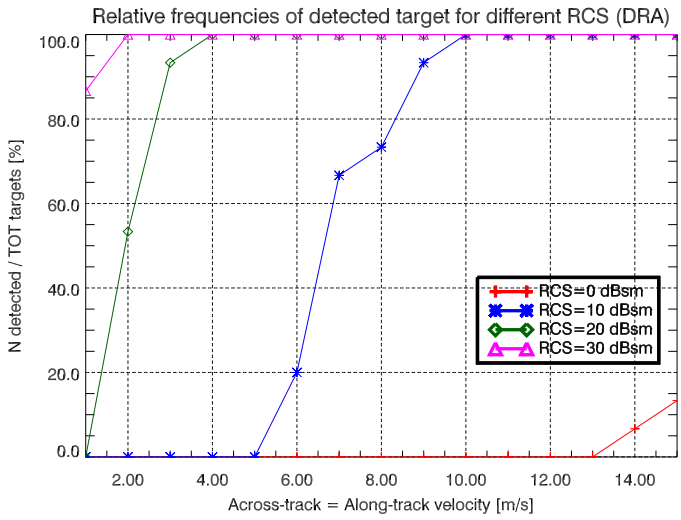

Figure 5.9: Relative frequencies of detected targets moving both with positive *across*-track and *along*-track velocity component for the Dual Antenna Receive mode of operation. The relative frequencies are plotted for different modeled boats, i.e. for different RCS values.

Toggle modes of operation

For the toggle modes of operation the probability of detection relative to the across-track equal to along-track velocity and for baselines of 0.6 m and 1.2 m for the three and four virtual channels is given respectively in figure 5.10 and 5.11.

Looking at these figures is noted that there is a degradation on the performance with respect to the two real channel case (DRA). As predictable by the SCNR plots, once again is understood that the toggle mode in a system with PAZ like parameter are not very useful, probably it could be possible to adjust the system to have increased energy consumption or optimize it to operate in these modes or work with a reduced resolution and reduced bandwidth to keep the SNR higher.

5.4 Velocity estimation

For the targets that are detected it is possible to estimate their across-track and along-track velocity. The estimation is carried out following the procedures explained in chapter 4 and using the same raw data generated to

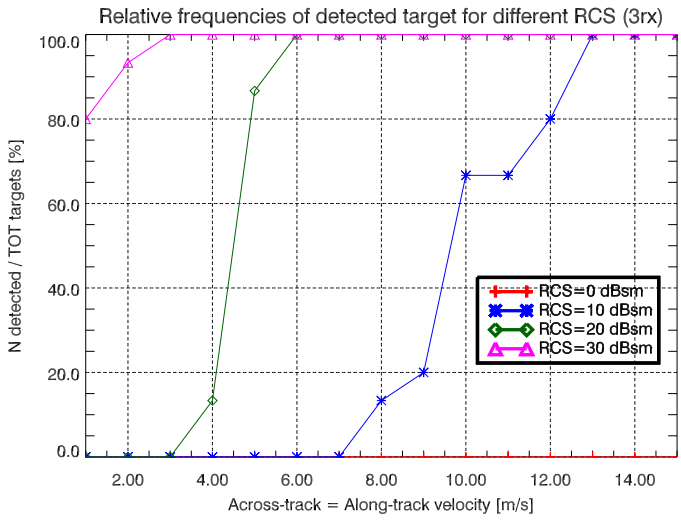

Figure 5.10: Relative frequencies of detected targets moving both with positive *across*-track and *along*-track velocity component for the toggle *three* virtual channels mode of operation. The relative frequencies are plotted for different modeled boats, i.e. for different RCS values.

calculate the experimental probability of detection illustrated in the preceding section.

In the successive tables from 5.4 to 5.6 the velocity estimation results are presented in terms of mean velocity, over the different trials. The minimum and maximum values are also reported in order to give an indication on the range of estimation error in case of considering only one trial.

To be easily readable it is preferred giving the tablesjust for the range between 2 and 14 m/s with a step of 2 m/s. The reader will not find the velocity estimation results for a small boat of RCS equal to 0 dBsm because it is practically undetectable, as seen in the previous section.

About the goodness of the measurements it is important to observe that in the case of high SCNR the target velocity estimation averaged on approximatively all the targets (30). On the contrary, in the case of small RCS values or slow velocity the average is obviously performed only for the detected target, for sure less than 30.

DRA across-track velocity

Tables 5.4 reports the results for the *across*-track velocity estimation for the DRA mode of operation extracted as explained in chapter 4 from the ATI

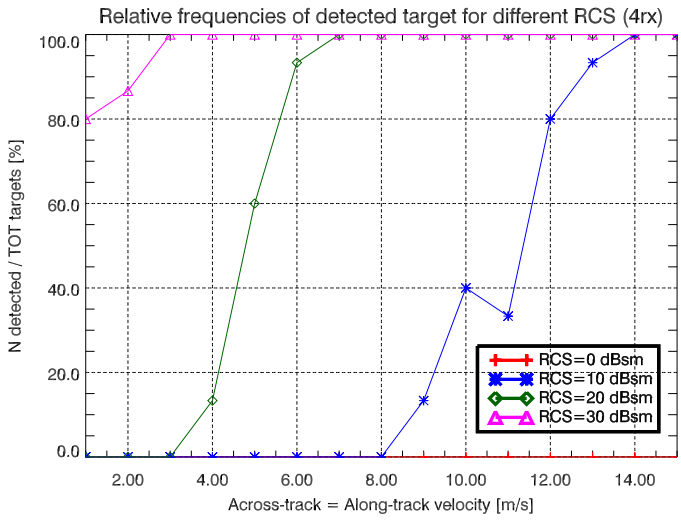

Figure 5.11: Relative frequencies of detected targets moving both with positive *across*-track and *along*-track velocity component for the toggle *four* virtual channels mode of operation. The relative frequencies are plotted for different modeled boats, i.e. for different RCS values.

phase. In the case of 10 dBsm and real velocity of 6 m/s it is clearly noted that the estimated velocity is biased. Despite this the estimated velocities for that RCS are quite good, with errors oscillating from 0.3 to 1.4 m/s. In the case of the RCS of 20 dBsm the maximum error in the mean value is always below 0.5 m/s for all the velocities taken into account. In the last case of across-velocity and a RCS of 30 dBsm the error in the mean value is always lower than 0.1 m/s. These results indicates that the bias error decreases with increasing dimension of the boats, i.e. increasing RCS and SCNR.

DRA along-track velocity

Table 5.5 reports the results for the *along*-track velocity estimation for the DRA mode of operation. In the case of 10 dBsm the error in the mean value is always lower than 2 m/s. In the case of the RCS of 20 and 30 dBsm the maximum error in the mean value is always below 0.8 m/s for all the velocities taken into account. The fact that there is no a significant improving from the 20dBsm to 30 dBsm is probably related to how the estimation is performed. As discussed in the section 4.3, the optimum fractional domain is the one in which is found the peak of maximum magnitude varying the rotational angle α. This rotational angle is used for the estimation of the along-track

(a) Target with RCS = 10 dBsm.

Real v.	2.0	4.0	6.0	8.0	10.0	12.0	14.0
mean	-	-	8.3	8.9	11.4	12.3	13.0
min	-	-	8.1	6.0	8.3	8.9	10.6
max	-	-	8.5	13.9	15.3	17.1	15.5

(b) Target with RCS = 20 dBsm

Real v.	2.0	4.0	6.0	8.0	10.0	12.0	14.0
mean	2.5	4.4	6.1	8.0	10.3	12.1	13.7
min	1.9	3.7	5.3	7.2	9.4	11.0	12.7
max	3.5	5.8	7.0	8.9	11.4	13.4	14.6

(c) Target with RCS = 30 dBsm

Real v.	2.0	4.0	6.0	8.0	10.0	12.0	14.0
mean	2.1	4.1	6.0	8.0	10.1	12.0	13.9
min	1.9	3.9	5.8	7.7	9.8	11.7	13.6
max	2.4	4.2	6.2	8.3	10.4	12.4	14.2

Table 5.4: Simulation results for the estimation of the *across*-track velocity component in the case of **Dual Antenna Receive** mode for different modeled boats (different RCS). The averaged, minimum and maximum values for different trials are given. The symbol '-' indicates that no targets were detected.

velocity. Therefore, the precision in the along-track velocity estimation is directly connected with the sensitivity to find small changes in the peak magnitude for the numerically calculated fractional Fourier transform, for different rotational angles.

Considerations on toggle modes velocity estimation

For completeness, in table 5.6 the simulation results for the three channel toggle modes for across and along-track velocity estimation are reported. For the across-track component the phase of the ATI is calculated from two DPCA and fractional domain filtered signals, the first DPCA is between channel 1 and 3 and the second between channel 3 and 2. The results are reported only for the case of RCS = 20 dBsm. It is possible to see that in comparison to the table 5.4 for the same RCS but in DRA mode of operation there is a deterioration in the estimation of the across-track component, once again the reasons lie in the loss of SCNR because of the half pulse duration

(a) Target with RCS = 10 dBsm

Real v.	2.0	4.0	6.0	8.0	10.0	12.0	14.0
mean	-	-	4.1	9.4	11.6	12.9	15.2
min	-	-	0.2	5.9	7.2	10.9	12.6
max	-	-	9.0	14.6	15.4	17.7	20.2

(b) Target with RCS = 20 dBsm

Real v.	2.0	4.0	6.0	8.0	10.0	12.0	14.0
mean	2.0	4.7	6.4	8.1	11.5	12.5	14.8
min	0.0	-0.5	0.6	4.5	9.0	10.0	12.7
max	5.0	10.6	9.6	9.9	14.3	14.2	17.2

(c) Target with RCS = 30 dBsm

Real v.	2.0	4.0	6.0	8.0	10.0	12.0	14.0
mean	2.7	4.7	6.8	8.2	11.4	12.5	14.8
min	-1.6	1.6	4.5	5.0	9.3	9.7	12.6
max	6.4	7.0	8.5	9.8	14.0	14.2	17.2

Table 5.5: Simulation results for the estimation of the *along*-track velocity component in the case of **Dual Antenna Receive** mode for different modeled boats (different RCS). The averaged, minimum and maximum values for different trials are given. The symbol '-' indicates that no targets were detected.

used for the virtual channels. The estimation of the along-track component is similar to the DRA case, this suggest that the search for the optimal rotational angle for the fractional Fourier transform seems to be more robust to noise with respect to calculation of the phase of the ATI for velocity estimation.

(a) Across-track velocity component estimation.

Real v.	2.0	4.0	6.0	8.0	10.0	12.0	14.0
mean	-	4.8	8.7	5.8	9.7	12.1	14.8
min	-	-9.2	-7.2	-6.9	-8.9	2.1	6.8
max	-	22.5	17.9	15.7	17.3	20.0	25.9

(b) Along-track velocity component estimation.

Real v.	2.0	4.0	6.0	8.0	10.0	12.0	14.0
mean	-	4.0	5.7	7.3	10.5	11.5	13.9
min	-	0.2	3.6	4.3	8.1	8.7	11.7
max	-	7.8	7.6	8.8	13.5	13.4	16.5

Table 5.6: Simulation results for the estimation of the along-track and across-track velocity component in the case of **toggle mode** of operation with three virtual channels. The values are for a target with RCS = 20 dBsm. The averaged, minimum and maximum values for different trials are given. The symbol '-' indicates that no targets were detected.

Conclusions

This thesis is born in the framework of satellites with synthetic aperture radar for maritime surveillance of moving ships.

The aim of the work was to implement, in the simulator under development at the UPC, some procedures for detection and velocity estimation of moving target. In particular, attention has been given on the possibility to perform the detection in the fractional Fourier domain, after clutter reduction by DPCA. Furthermore, the creation of additional virtual channels has been considered by means of programming of the antenna in receive. Finally, to test the goodness of the proposed techniques, several simulations have been carried out considering SAR parameters similar to the future Spanish SEOSAR/PAZ satellite.

Detection

The results obtained with regard to the detection, confirm that it is possible to accomplish Ground Moving Target Detection in the fractional domain. It is known that in the classic GMTI techniques, based on a DPCA operation in compressed data, fast along-track moving target appear defocused. Also deteriorating the output SCNR. In the fractional domain this fact does not occurs and has been confirmed by means of the simulation both with the SCNR and with the probability of detection. In the range of velocities of interest, the faster is a boat and more it is detectable. A small inflatable boat, modeled with a RCS of 0 dBsm was nearly undetectable in all the simulations. For a small fishing boat moving more than 9 m/s results that it is practically always detected, same consideration are made for a vessel that moves at speed higher than 3 m/s. For smaller velocities the detection results effective only for big ships.

Velocity estimation

Concerning the across-track component of the velocity it can be stated that it is estimated with an error of about 3 m/s in the case of small boats. For bigger boats the error is around 1 m/s.

With respect to the along-track component, exploiting the value of the angle of the optimum fractional domain, are found error around 4 m/s for small boats and of 2 m/s for bigger ships. The main contribution of this thesis arise making a comparison between the proposed method and the filter bank technique previously used in the UPC simulator. In fact, results that the along-track velocities are estimated with a better accuracy measurable in about 5 m/s.

In conclusion the estimation of both the across and the along-track component is effective and allow to localize the target in a limited area.

Toggle modes

Regarding the toggle modes of operation the conclusion is that if it is required to maintain the same power consumption of the standard operational mode (hence halving the energy-per-pulse) the performance, with the proposed technique, for both detection and estimation are worst than considering the standard two channel receiving mode. Probably it could be adjust the system to have increased energy consumption or optimize it to operate with these toggle modes. It is also possible to operate these modes with a bigger antenna and where the SNR conditions are not so restrictive as in the case considered in this thesis.

Future works

If the interest is to build a less complicated system it can be thought to significantly simplify the proposed algorithm in this thesis but preserving its fine ability to estimate the along-track velocity component. The idea is to perform the fractional transform for along-track velocity estimation only for the lines where moving targets were detected using a classic DPCA CFAR detector, or a 2-dimensional ATI detector.

The UPC SAR-MTI simulator is being updated with a more realistic sea clutter model based on a K-distribution. Also the accelerations should be taken into account to realize a more realistic model of boat moving in an wavy sea.

In the wide context of SAR-GMTI systems it should be noted that are been investigating ways to have more degrees of freedom for weak target

detection and its velocity estimation. Apart from the toggle mode, multi-static systems formed by satellites constellations or solution with folded or extendable antenna are promising alternatives.

Bibliography

[1] Love, A.; "In memory of Carl A. Wiley", Antennas and Propagation Society Newsletter, IEEE , vol.27, no.3, pp.17-18, June 1985

[2] Moccia, A.; Rufino, G. ; "Spaceborne along-track SAR interferometry: performance analysis and mission scenarios", Aerospace and Electronic Systems, IEEE Transactions on , vol.37, no.1, pp.199-213, Jan 2001

[3] `http://earth.esa.int/applications/data_util/SARDOCS`

[4] Burini, A.; Schiavon, G.; "RADARSAT-2: Main features and near real-time applications" Radar Conference, 2009. EuRAD 2009. European , vol., no., pp.153-155, Sept. 30 2009-Oct. 2 2009

[5] Hajnsek, I.; Eineder, M.; , "TerraSAR-X: science exploration of polarimetric and interferometric SAR," Geoscience and Remote Sensing Symposium, 2005. IGARSS '05. Proceedings. 2005 IEEE International , vol.7, no., pp. 4882- 4885, 25-29 July 2005

[6] Di Lazzaro, M.; Angino, G.; Piemontese, M.; Capuzi, A.; Leonardi, R. "COSMO-SkyMed: The Dual-Use Component of a Geospatial System for Environment and Security" Aerospace Conference, 2008 IEEE , vol., no., pp.1-10, 1-8 March 2008

[7] Gonzalez, A.S.; Labriola, M.; Soteras, J.C.; Palma, J.S. "PAZ instrument design and performance," Synthetic Aperture Radar (APSAR), 2011 3rd International Asia-Pacific Conference on , vol., no., pp.1-4, 26-30 Sept. 2011

[8] Shen Chiu; Livingstone, C.; Sikaneta, I.; Gierull, C.; Beaulne, P. "Radarsat-2 Moving Object Detection Experiment (MODEX)" Geoscience and Remote Sensing Symposium, 2008. IGARSS 2008. IEEE International , vol.1, no., pp.I-13-I-16, 7-11 July 2008

[9] Topputo F., "Monitoraggio via Satellite dei Flussi Migratori nell'Area del Mediterraneo" Rapporto di Ricerca Ce.Mi.S.S., December 2009

[10] "Space research - Desire of space, Space research projects under the 7th Framework Programme for research", available at `http://ec.europa.eu/enterprise/policies/space/files/research/fp7_desire_for_space.pdf`

[11] S. Chiu, "A Simulation Study of Multi-Channel RADARSAT-2 GMTI", TECHNICAL MEMORANDUM DRDC Ottawa TM 2006-209, Defence R&D Canada, November 2006

[12] Ian G. Cumming; Frank H. Wong, "Digital Processing Of Synthetic Aperture Radar Data: Algorithms And Implementation" ,Artech House Remote Sensing Library, January 2005

[13] Mittermayer, J.; Runge, H., "Conceptual studies for exploiting the TerraSAR-X dual receive antenna," Geoscience and Remote Sensing Symposium, 2003. IGARSS '03. Proceedings. 2003 IEEE International , vol.3, no., pp. 2140- 2142, 21-25 July 2003

[14] Gierull, C.H.; "Ground moving target parameter estimation for two-channel SAR," Radar, Sonar and Navigation, IEE Proceedings - , vol.153, no.3, pp. 224- 233, June 2006

[15] Merrill I. Skolnik, "Radar Handbook", McGraw-Hill Publishing Co., 2nd Revised edition, 1989

[16] J.H.G. Ender; "Detection and estimation of moving target signal by multi-channel SAR", AEU-Int. J. Electron. Commun., 1996,50, pp. 150-156

[17] Suchandt, S. and Runge, H. and Steinbrecher, U., "Ship detection and measurement using the TerraSAR-X dual-receive antenna mode", Geoscience and Remote Sensing Symposium (IGARSS), 2010

[18] F. Lombardini, F. Bordoni, F. Gini, "Feasibility Study of Along-track SAR Interferometry with the COSMO-Skymed Satellite System", 2004

[19] Sharma J., "The influence of target acceleration on dual-channel SAR-GMTI (synthetic aperture radar ground moving target indication) data", Master thesis, Department of Geomatics Engineering, 2004

[20] Eduardo Makhoul, Antoni Broquetas, Oriol Gonzalez, "Evaluation of State-of-the-Art GMTI techniques for Future Spaceborne SAR Systems -Simulation Validation-", 2011

[21] Antipov I., "Simulation of Sea clutter returns, Tactical Surveillance Division and Electronic and Surveillance Research Laboratory", June 1998.

[22] F. Nathanson, J. Reilly, and M. Cohen, "Radar Design Principles - Signal Processing and the Environment", SciTech Pub., 1999. Sea clutter table chapter 7 p. 278

[23] S.J. Frasier, A.J. Camps, "Dual-beam Interferometry for Ocean Surface Current Vector Mapping.", IEEE Trans on Geosci. and Remote Sensing, 39 (2), pp. 401-414, Feb 2001.

[24] World Meteorological Organization Manual on Codes, No. 306, part A, Alphanumeric codes (WMO sea state Code, table 3700, p. A-326). Can be found in `http://www.wmo.int/pages/prog/www/WMOCodes.html#ManualCodes`

[25] World Meteorological Organization Manual on Codes, No. 306, part A, Alphanumeric codes (Section E, Beaufort Wind scale, p. A-379)

[26] White, R.G.; Coe, D.J.; , "Detection limits for sideways looking MTI radars," Radar 97 (Conf. Publ. No. 449) , vol., no., pp.434-438, 14-16 Oct 1997

[27] Ender, J.H.G., "Space-time processing for multichannel synthetic aperture radar" Electronics Communication Engineering Journal, feb. 1999

[28] Golikov, V.; Castillejos, A.; Lebedeva, O.; Ponomaryov, V.; Cruz-Irisson, M.; , "CFAR robust detection of moving target in presence of fluctuating background," Mathematical Methods in Electromagnetic Theory, 2008. MMET 2008. 12th International Conference on , vol., no., pp.144-146, June 29 2008-July 2 2008

[29] Dong, Zhen and Cai, Bin and Liang, Diannong, "Detection of Ground Moving Targets for Two-Channel Spaceborne SAR-ATI", EURASIP Journal on Advances in Signal Processing 1, 2010

[30] Shen Chiu, "A constant false alarm rate (CFAR) detector for RADARSAT-2 along-track interferometry", Canadian Journal of Remote Sensing, 2005, 31(1): 73-84, 10.5589/m04-057

[31] E. Makhoul, C. González, A. Broquetas, "Gaps Assessment: Required Techniques", D9 NEWA Project co-funded by the European Commission within the Seventh Framework Programme, January 2012

[32] C.E. Livingstone, I. Sikaneta, C.H. Gierull, S. Chiu, A. Beaudoin, J. Campbell, J. Beaudoin, S. Gong, and T.A. Knight, "An airborne synthetic aperture radar (SAR) experiment to support RADARSAT-2 ground moving target indication (GMTI)", Can. J. Remote Sensing, Vol. 28, No. 6, pp. 794-813, 2002

[33] C. González, "Detección y estimación de velocidad de objetivos móviles mediante radares de apertura sintética con configuración de canal dual (dual channel SAR)", master thesis at Universitat Politècnica de Catalunya, Spain

[34] Chiu, S. "Application of Fractional Fourier Transform to Moving Target Indication via Along-Track Interferometry" ,EURASIP Journal on Advances in Signal Processing,20, 2005

[35] Almeida, L.B.; , "The fractional Fourier transform and time-frequency representations ," Signal Processing, IEEE Transactions on , vol.42, no.11, pp.3084-3091, Nov 1994

[36] Baumgartner, S.V.; Krieger, G.; , "Acceleration-independent along-track velocity estimation of moving targets," Radar, Sonar & Navigation, IET , vol.4, no.3, pp.474-487, June 2010

[37] Sijbers J., den Dekker A. J., Raman E. and Van Dyck D., "Parameter estimation from magnitude MR images", International Journal of Imaging Systems and Technology, Vol. 10, Nr. 2, p. 109-114, (1999)

[38] E. Makhoul, "Synthetic aperture radar moving target indication simulator tool -user manual", UPC, september 2011

Un grazie infinito a mamma Elena e papà Nico perchè hanno sempre creduto nelle mie capacità ed hanno incondizionatamente sostenuto tutte le scelte che ho fatto. Grazie papà per le quotidiane bistecche che hai preparato per me in quest' ultima settimana e grazie mamma per le notturne tisane rilassanti, sembra che alla fine tutto ciò abbia funzionato!

Grazie sorellina perchè, nonostante la distanza che ci separa da due anni, nei momenti in cui ci ritroviamo a parlare sappiamo essere i due fratellini di sempre.

Un ringraziamento davvero sincero a tutti gli amici che mi sopportano. Non voglio fare l'elenco dei nomi, a ciascuno di voi dico che dopo questo tempo speso all' estero sento il bisogno di vederci e parlarci.

Semplicemente grazie alla mia Marty per la pazienza e perchè "lei gli raccontava le favole ... lui le insegnava a volare ..."

Voglio dire grazie a tutte le persone che ogni anno rendono possibile il progetto Erasmus per migliaia di studenti europei. Senza di esse sicuramente questa tesi non sarebbe mai esistita ed io probabilmente non avrei mai avuto la possibilita di legare il mondo degli studi con la mia passione per lo spazio.